mTOR complex 2-Akt signaling at mitochondria-associated endoplasmic reticulum membranes (MAM) regulates mitochondrial physiology

Charles Betz[a], Daniele Stracka[a], Cristina Prescianotto-Baschong[a], Maud Frieden[b], Nicolas Demaurex[b], and Michael N. Hall[a,1]

[a]Growth and Development, Biozentrum, University of Basel, CH-4056 Basel, Switzerland; and [b]Department of Cell Physiology and Metabolism, University of Geneva, 1211 Geneva 4, Switzerland

This Feature Article is part of a series identified by the Editorial Board as reporting findings of exceptional significance.

Edited by Tony Hunter, The Salk Institute for Biological Studies, La Jolla, CA, and approved May 24, 2013 (received for review February 6, 2013)

The target of rapamycin (TOR) is a highly conserved protein kinase and a central controller of growth. Mammalian TOR complex 2 (mTORC2) regulates AGC kinase family members and is implicated in various disorders, including cancer and diabetes. Here we report that mTORC2 is localized to the endoplasmic reticulum (ER) subcompartment termed mitochondria-associated ER membrane (MAM). mTORC2 localization to MAM was growth factor-stimulated, and mTORC2 at MAM interacted with the IP_3 receptor (IP3R)-Grp75–voltage-dependent anion-selective channel 1 ER-mitochondrial tethering complex. mTORC2 deficiency disrupted MAM, causing mitochondrial defects including increases in mitochondrial membrane potential, ATP production, and calcium uptake. mTORC2 controlled MAM integrity and mitochondrial function via Akt mediated phosphorylation of the MAM associated proteins IP3R, Hexokinase 2, and phosphofurin acidic cluster sorting protein 2. Thus, mTORC2 is at the core of a MAM signaling hub that controls growth and metabolism.

Mitochondria-associated endoplasmic reticulum (ER) membrane (MAM) is a subcompartment of the ER that forms a quasisynaptic structure with mitochondria. The main function of this membrane is to facilitate the transfer of lipids and calcium between the two organelles. MAM thereby controls mitochondrial physiology and apoptosis (1, 2). MAM also mediates ER homeostasis and lipid biosynthesis by harboring chaperones and several key lipid synthesis enzymes (3–6). In mammalian MAM, the ER and mitochondria are physically tethered to each other by the IP_3 receptor (IP3R)-Grp75-VDAC1 (voltage-dependent anion-selective channel 1) trimeric complex (7) and by dimers of the mitofusin (Mfn) proteins Mfn1 and Mfn2 (8) (Fig. S1*H*). The σ-1 receptor also stabilizes MAM by interacting with IP3R and VDAC (9). MAM formation is regulated by multiple signaling inputs, including calcium and possibly growth factors (10–12). However, the mechanism(s) that controls MAM formation is largely unknown other than it involves recruitment of MAM components by the MAM resident proteins phosphofurin acidic cluster sorting protein 2 (PACS2) and Rab32 (13–15). Akt, an AGC family kinase that is also found at MAM (16), phosphorylates PACS2 (17), but it remains to be determined whether Akt is involved in mediating MAM integrity.

Akt, often up-regulated in cancer, also phosphorylates hexokinase 2 (HK2) to promote association of HK2 with the MAM protein VDAC1 (18, 19). This association, possibly at MAM (20, 21), enables HK2, using ATP exiting mitochondria through VDAC1, to phosphorylate glucose and thereby stimulate glycolysis (22). Conversely, upon inhibition of Akt, HK2 dissociates from VDAC1, causing VDAC1 closure and increased mitochondrial membrane potential (19). This regulation of HK2 by Akt has been proposed to account for enhanced glycolysis in cancer cells, also known as the Warburg effect (23). Furthermore, Akt regulates calcium release from MAM by phosphorylating IP3R, thereby controlling apoptosis (24–26). Thus, MAM is increasingly recognized as a signaling hub controlling cell physiology (15), and is implicated in a wide spectrum of diseases, including cancer, neurodegenerative disorders, inflammation, and infection (27).

The target of rapamycin (TOR) pathway is a cellular signaling cascade that, like mitochondria, is present in all eukaryotes (28, 29). TOR integrates and relays signals from both extra- and intracellular sources (e.g., growth factors, nutrients, and cellular energy levels), and thereby instructs the cell to grow. TOR is found in two structurally and functionally distinct protein complexes that in mammalian cells are termed mTOR complex 1 (mTORC1) and mTOR complex 2 (mTORC2) (30). mTORC2 comprises mTOR, rictor, mammalian lethal with SEC13 protein 8 (mLST8), stress-activated protein kinase (SAPK)-interacting protein (Sin1), and protor [also known as proline-rich protein 5 (PRR5)] (31), and phosphorylates AGC kinases, such as Akt, serum/glucocorticoid-regulated kinase 1 (SGK1), and PKC, all of which are linked to cancer and diabetes (32). Growth factors activate mTORC2 by promoting mTORC2-ribosome association in a PI3K-dependent manner (33, 34). mTORC2 is antiapoptotic, presumably via its role in phosphorylating and activating Akt (34–38).

Various observations indicate that mTORC2 is linked to both the ER and mitochondria. Recent findings suggest that mTORC2 is at the ER, possibly through interaction with ER-bound ribosomes (34, 39). mTORC2 phosphorylates Akt at the ER (39, 40), and mTORC2 signaling is sensitive to ER stress (41, 42). In *Chlamydomonas*, TOR associates with membranes from the ER (43). With regard to mitochondria, mTOR has been observed in close proximity to the outer mitochondrial membrane (44), and mTOR and mLST8 interact with the mitochondrial outer-membrane protein VDAC1 (45) and the mitochondria-associated protein Grp75 (46), respectively. mTORC2 regulates the cellular distribution of mitochondria (47), and mTORC2-activated Akt is associated with mitochondria (18, 48, 49). Pink1, a regulator of mitochondrial function, has been implicated in mTORC2 activation (50). mTORC2-addicted cancer cells exhibit enhanced dependence on mitochondria, Rab32 and HK2 (51). Finally, Barquilla et al. reported that TORC2 in trypanosomes is localized to both ER and mitochondria (52). Thus,

Author contributions: C.B., N.D., and M.N.H. designed research; C.B., C.P.-B., and M.F. performed research; C.B. analyzed data; D.S. and N.D. contributed new reagents/analytic tools; and C.B. and M.N.H. wrote the paper.

The authors declare no conflict of interest.

This article is a PNAS Direct Submission.

Freely available online through the PNAS open access option.

[1]To whom correspondence should be addressed. E-mail: M.Hall@unibas.ch.

This article contains supporting information online at www.pnas.org/lookup/suppl/doi:10.1073/pnas.1302455110/-/DCSupplemental.

mTORC2 has been physically and functionally linked to both the ER and mitochondria.

Here we investigate the localization of mTORC2. We show that ribosome-bound mTORC2 is at MAM. Localization to MAM is growth factor-dependent. MAM-associated mTORC2 activates Akt and thereby controls MAM integrity, mitochondrial metabolism, and cell survival. Thus, our findings describe a critical role for mTORC2 in a MAM signaling hub.

Results

mTORC2 Localizes to Mitochondria-Associated ER-Membranes. To examine mTORC2 localization, we isolated ER from mouse liver extracts by isopycnic flotation (53). Liver was used because it is a rich source of ER and because previous studies on mTORC2 localization were performed only with cultured cells. Twenty to 60% of mTORC2 (Sin1 and rictor) was ER-associated in liver cells. mTORC1 (raptor) was not detected in the ER fraction from liver cells (Fig. 1*A*). Sin1 in the ER fraction coimmunoprecipitated with mTOR, rictor, and the ribosome, confirming that mTORC2 at the ER is intact and associated with ribosomes (Fig. 1*B*). Thus, mTORC2 appears to be localized to the ER.

To characterize further the subcellular localization of mTORC2, we analyzed rictor and Sin1 localization by indirect immunofluorescence. The mTORC2 signal overlapped with ER adjacent to mitochondria (Fig. 1*C* and Fig. S1 *A* and *B*), a staining pattern similar to that observed for MAM-localized proteins (15, 54, 55). Controls indicating the validity of the rictor and Sin1 antibodies for immunofluorescence are presented in Fig. S1 *C* and *D*. We also detected rictor in close proximity to both the ER and mitochondria by immuno-electron microscopy (EM) on mouse liver and HEK293T cells (Fig. 1*D* and Fig. S1*E*). In HEK293T cells, 38% (±3.9) of rictor was adjacent to mitochondria and 48%

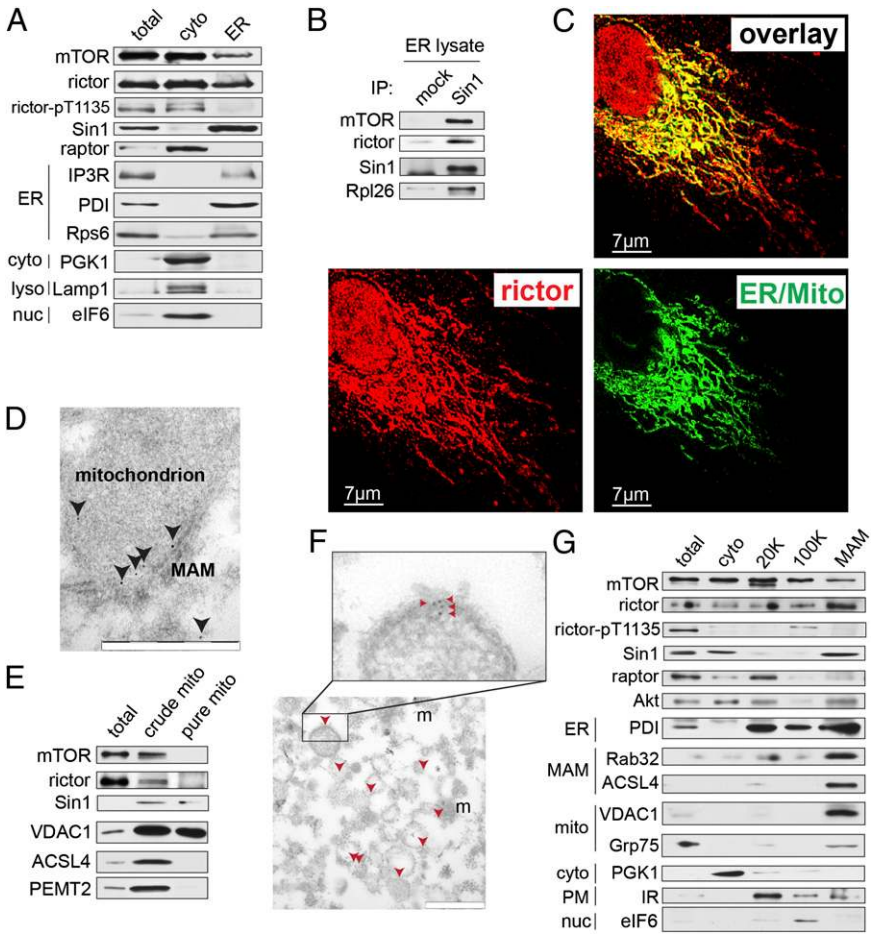

Fig. 1. mTORC2 is localized to MAMs. (*A*) mTORC2 components are present in the ER fraction of mouse livers. Total, whole cell lysate; cyto, cytoplasmic extract; ER, heavy membrane fraction from isopycnic flotation. Lysates were pooled from three different mouse livers. Mice were fed a standard chow diet and killed in the morning. Equal total protein levels were loaded in each lane. (*B*) mTORC2 in mouse liver ER extracts is intact and ribosome-associated. ER fraction was prepared as in *A*, suspended in CHAPS IP buffer and mTORC2 components were coimmunoprecipitated with Sin1. (*C*) ER/mito staining, reflecting colocalized ER (ER-GFP) and mitochondria (Mito-RFP), overlaps with endogenous rictor signal in U2OS cells. For individual channels, see Fig. S1*A*. (Scale bar, 7 μm.) Shown is maximum-intensity projection of 3D-deconvoluted, confocal image stack. Cells were grown on coverslips in normal medium before PFA fixation. (*D*) Representative image showing rictor (arrowheads) localization at the rough ER (electron-dense tubular structure) adjacent to a mitochondrion in a mouse liver section as detected by immuno-EM. (Scale bar, 500 nm.) (*E*) mTOR and rictor can be detected in crude mitochondrial extracts from mouse liver cells but not in purified mitochondrial extracts. Lysates were pooled from three different mouse livers. Mice were fed a standard chow diet and killed in the morning. Equal total protein levels were loaded in each lane. (*F*) Rictor (red arrowheads) is present in a purified MAM fraction as measured by immuno-EM. Rictor signal is localized to the surface of reconstituted microsomes consisting of pure MAM membranes (56); m, mitochondrion, copurified with MAM. (Scale bar, 500 nM.) (*G*) Purified MAM fraction from mouse liver extracts contains mTORC2 components but not mTORC1 component raptor. MAM markers include Rab32 and ACSL4, cytosolic marker is PGK1 mitochondrial markers are VDAC1 and Grp75, ER marker is PDI, plasma membrane marker is the insulin receptor (IR), and nuclear marker is eIF6. Lysates are pooled from three different mouse livers. 20 K and 100 K indicate fractions as described in ref. 56. Mice were fed a standard chow diet and killed in the morning. Equal total protein levels were loaded in each lane.

(±4.7) was cytoplasmic (Fig. S1*F*). Thus, mTORC2 appears to be localized to the ER subdomain MAM.

We next examined further whether mTORC2 is MAM-associated. First, as assayed by immunoblotting of subcellular preparations, rictor was detected in a crude mitochondria fraction but not in a fraction of pure mitochondria that had been stripped of peripheral MAM (56) (Fig. 1*E*). Second, as assayed by immuno-EM on purified MAM, rictor displayed a pattern (Fig. 1*F*) similar to that observed previously for the established MAM marker phosphatidyl ethanolamine methyltransferase (PEMT)2 (57). Third, ∼15% of total Sin1 and rictor was detected in a purified MAM fraction (Fig. 1*G*). Finally, we observed that rictor, but not the mTORC1 component raptor, coimmunoprecipitated with components of the MAM tethering complex IP3R-Grp75-VDAC1 (Fig. S1*G*). Thus, mTORC2 localizes to the ER subcompartment MAM, consistent with a recent proteomic study that identified mTOR at MAM (21).

Localization of mTORC2 to MAM Is Stimulated by Growth Factors. Previous studies have suggested that mTORC2 phosphorylates Akt at the ER (39, 40). Because mTORC2 activity is insulin-PI3K stimulated, we examined whether localization of mTORC2 to MAM is regulated by growth factors. First, we observed higher levels of mTORC2 (rictor) at MAM in wild-type but not rictor knockout (KO) mouse embryonic fibroblasts (MEFs) upon insulin stimulation (Fig. 2*A*). Elevated levels of mTORC2 (rictor, Sin1) were also detected at MAM in liver extracts of mice starved overnight and refed for 2 h (Fig. 2 *B* and *C*, and Fig. S2*A*). Second, we detected enhanced interaction between mTORC2 and the MAM tethering complex IP3R-Grp75-VDAC1 after insulin stimulation (Fig. 2*D* and Fig. S2*B*), as assayed by coimmunoprecipitation. Finally, by immunofluorescence, we observed a significant increase in colocalization of rictor with mitochondria (Fig. 2*E* and Fig. S2*F*) in cells grown in the presence of serum, compared with serum-starved cells. Thus, localization of mTORC2 to MAM is stimulated by growth factors.

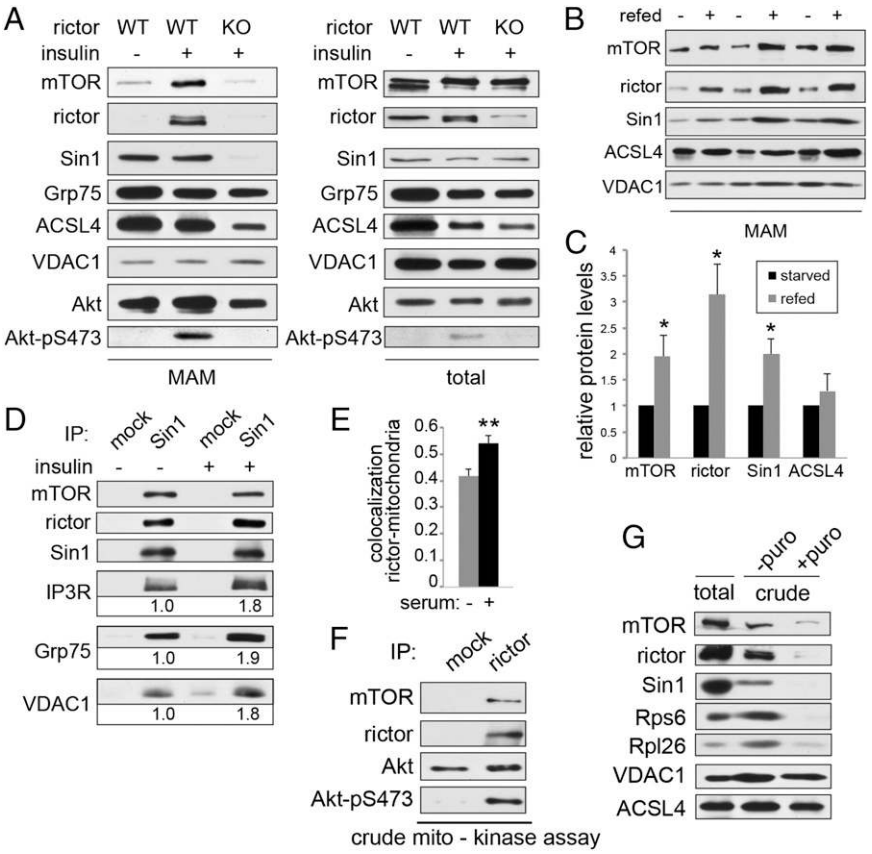

Fig. 2. mTORC2 localization to MAM is stimulated by growth factors. (*A*) mTORC2 localization to MAM is increased in insulin-stimulated control MEFs but not in MEFs in which rictor KO had been induced by addition of tamoxifen before the experiment. MEFs were starved for 6 h before the experiment and stimulated for 30 min using 100 nM insulin. MAM was isolated as before. Five confluent 15-cm plates were used as starting material for each condition. (*B*) mTORC2 localization to MAM is increased in livers of refed control mice, indicating that increased mTORC2 localization to MAM is also observed under physiological stimulation by food intake. Mice were starved for 14 h and refed standard diet for 2 h. Two mice were used for each fractionation. (*C*) Densitometric quantification of *B*. Protein levels were normalized to VDAC1 signal. Note that ACSL4 levels are unchanged between starved and refed status as a result of loading of equal amount of MAM. (*D*) mTORC2 interaction with IP3R-Grp75-VDAC1 is increased after insulin stimulation in total liver extracts from insulin-stimulated control mice. Proteins were quantified relative to starved state. Mice were starved for 14 h and injected intraperitoneally with 4.5 mg/kg insulin or saline 30 min before being killed. Liver tissue was homogenized in CHAPS IP buffer. (*E*) Rictor colocalization (Pearson's coefficient) with mitochondria is increased in presence of serum in U2OS cells. Quantification of Fig. S2*F* ($n = 12$). (*F*) mTORC2, immunoprecipitated from a crude mitochondrial fraction purified from mouse liver lysates as previously, is active toward recombinant, kinase-dead Akt in an mTORC2 kinase assay. Lysates from two mice were combined for subcellular fractionation. Mice were starved for 14 h before being killed and injected intraperitoneally with 4.5 mg/kg insulin 15 min before being killed. (*G*) Stripping off ribosomes from crude mitochondrial extracts leads to a decrease of copurifying mTORC2 components, indicating that localization of mTORC2 to MAM depends on the presence of ribosomes. Crude mitochondrial extracts (including MAM) from HeLa cells were treated with 1 mM puromycin for 1 h and repurified. Note the decrease in the amount of ribosomes and mTORC2 but not in the mitochondrial marker VDAC1 or the MAM marker ACSL4. HeLa cells were growing in normal medium before the extraction. Results are shown as mean ± SEM and normalized to control cells. $*P < 0.05$, $**P < 0.01$.

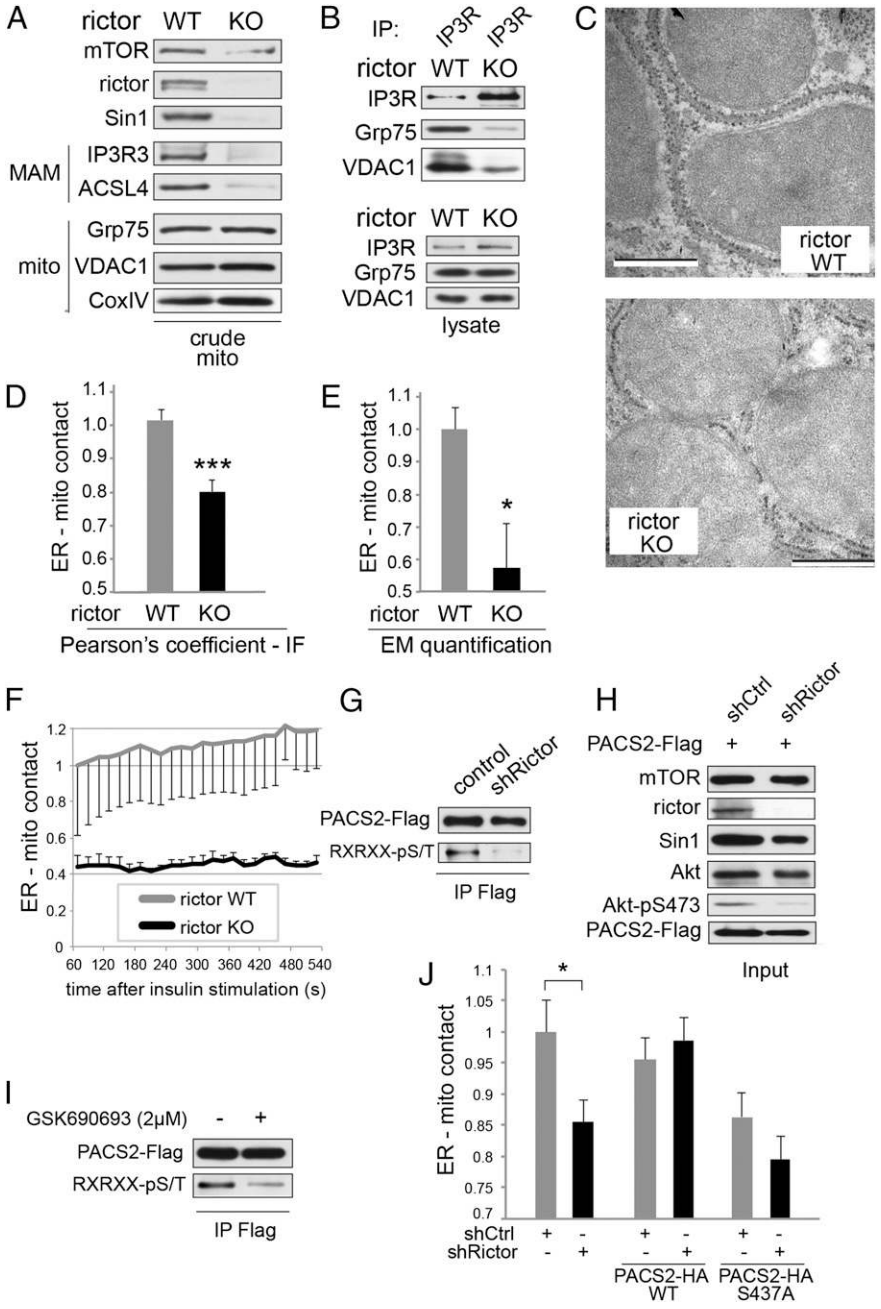

Fig. 3. mTORC2 mediates MAM integrity. (*A*) Inducible rictor KO MEFs show reduced amount of MAM markers IP3R3 and ACSL4 in crude mitochondrial extracts, indicating a reduction in MAM integrity. Rictor KO in MEFs was induced by a 4-d tamoxifen treatment of Rictor fl/fl CreERT2 MEFs (72) in this panel and in subsequent experiments. Cells were grown in normal medium before harvest. Equal total proteins were loaded in each lane, thus allowing us to judge the dynamic amount of MAM relative to the static amount of mitochondria in the crude mitochondrial fraction. Corresponding total protein lysates are shown in Fig. S3*A*. (*B*) Immunoprecipitation of IP3R from total liver extracts of rictor KO mice show reduced interaction of IP3R with VDAC1 and Grp75, indicating MAM disruption. Mice were fed a standard chow diet and killed in the morning. Input is shown in the lower panel. Immunoprecipitation was performed in CHAPS IP buffer as before. (*C*) High-magnification electron micrographs of liver mitochondria and surrounding MAM from liver-specific rictor KO mice and control littermates. (Scale bar, 500 nm.) Mice were fed a standard chow diet and killed in the morning. (*D*) Pearson's correlation coefficient quantifying 3D ER-mitochondrial contact of deconvoluted confocal image stacks of rictor KO relative to control (WT) MEFs. Cells expressed GFP-ER and mRFP-mito (BACMAM 2; Invitrogen). Quantification of Fig. S3*C*. $n = 9$. Cells were grown on coverslips in normal medium before PFA fixation. (*E*) Quantification of ER-mitochondrial contact of EM pictures from livers of liver-specific rictor KO mice and control littermates, $n = 6$. Mice were fed a standard chow diet and killed in the morning. (*F*) Life cell quantification of ER-mitochondrial contact of MEFs after stimulation with insulin, quantified by confocal microscopy as done previously ($n = 8$). Cells were grown on chambered coverglass (Lab-Tek) in normal medium, serum-starved for 6 h, and insulin-stimulated (100 nM) at $t = 0$. (*G*) Rictor knockdown HeLa cells show reduced phosphorylation of PACS2 at Akt target site. PACS2-Flag was immunoprecipitated and probed with a Flag-tag or an Akt substrate motif antibody. For input, see *H*. Thirty-four hours after PACS2 transfection, cells were serum-starved for 14 h, stimulated with insulin (100 nM) for 15 min, and lysed in RIPA buffer. (*H*) Input of *G*. (*I*) GSK690693 (an Akt ATP-competitive kinase inhibitor) treatment of HeLa cells inhibits phosphorylation of PACS2 at Akt target site. PACS2-Flag was immunoprecipitated and probed with a Flag-tag or an Akt substrate motif antibody. Thirty-four hours after PACS2 transfection, cells were serum-starved for 14 h, pretreated with the inhibitor or DMSO for 20 min, and stimulated with insulin (100 nM) for 15 min in the presence or absence of inhibitor. Cells were lysed in RIPA buffer. For input, see Fig. S3*J*. (*J*) ER-mitochondrial contact of rictor knockown or control HeLa cells transfected either with mock, PACS2-WT, or PACS2-S473A, quantified by immunofluoresence as done previously ($n = 10$–16). Cells were grown on coverslips in normal medium before fixation by PFA. Results are shown as mean ± SEM and normalized to control cells. $^{*}P < 0.05$, $^{***}P < 0.001$.

Because activation of mTORC2 involves binding to the ribosome, we examined whether mTORC2 at MAM is active and whether MAM localization of mTORC2 requires ribosome binding. First, we detected S473-phosphorylated Akt, the main read-out of mTORC2 activity, in MAM fractions (Fig. 2*A* and Fig. S2*A*). Second, MAM-associated mTORC2 was active against recombinant Akt in an mTORC2 kinase assay in vitro (Fig. 2*F*). Third, as judged by coimmunoprecipitation from whole-cell extracts, the interaction between mTORC2 and its substrate Akt was reduced in MAM-deficient Mfn1/2 double-KO MEFs, suggesting that MAM is an important site of mTORC2-Akt interaction (Fig. S2 *D* and *E*). Finally, stripping ribosomes from crude mitochondria (Fig. 2*G*) (consisting of mitochondria and MAM) reduced the amount of mTORC2 in these subcellular fractions. Ribosomes were stripped from the isolated organelles by treatment with puromycin; the stripping was thus specific for ribosomes (58). The above observations together suggest that localization of mTORC2 to MAM and subsequent activation are dependent on growth factor signaling and interaction with the ribosome.

mTORC2 Mediates MAM Integrity. Is mTORC2 localization to MAM functionally relevant, as suggested by our above observations that mTORC2 and mTORC2-phosphorylated Akt are present at MAM (Fig. 2*A*)? To answer this question, we examined whether mTORC2 is required for MAM integrity. First, we investigated the amounts of the MAM proteins IP3R and acyl CoA synthetase 4 (ACSL4) in a crude mitochondrial fraction, a technique previously established to quantify MAM (8). The amounts of IP3R and ACSL4 were reduced in a crude mitochondrial fraction from rictor KO MEFs and livers compared with wild-type cells (Fig. 3*A* and Fig. S3 *A* and *B*), while total IP3R levels were unchanged (Fig. S4 *A* and *B*). As a second method to assay MAM integrity (7, 8), we investigated the IP3R-Grp75-VDAC1 complex. Less Grp75 and VDAC1 coimmunoprecipitated with IP3R in rictor KO cells (Fig. 3*B*). Third, we quantified MAM integrity by analysis of 3D confocal images of cells coexpressing fluorescent probes for the ER and mitochondria (8, 13, 15, 54). Rictor, Sin1, and Akt1 KO cells exhibited reduced ER-mitochondrial contact (Fig. 3*D* and Fig. S3 *C*–*E*). Fourth, to

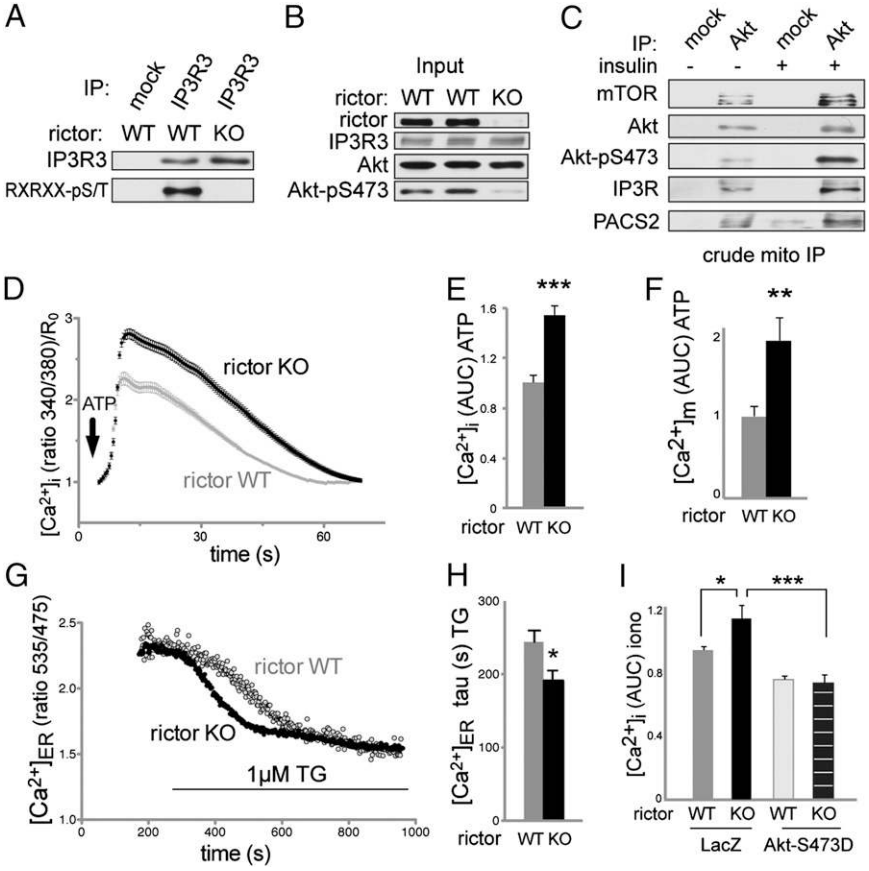

Fig. 4. Calcium flux is defective in mTORC2 deficient cells. All calcium measurements were performed in the absence of extracellular calcium. (*A*) Phosphorylation of endogenous IP3R3 is reduced in rictor KO MEFs. For input, see *B*. Cells were serum-starved for 14 h and stimulated with 100 nM insulin for 30 min before harvest in CHAPS IP buffer. (*B*) Input of *A*. (*C*) Immunoprecipitation of Akt from a crude mitochondrial fraction of mouse liver extracts. Mice were starved for 14 h and injected intraperitoneally with 4.5 mg/kg insulin or saline 15 min before being killed. Lysates from three mice were pooled for subcellular fractionation. IP was performed in CHAPS IP buffer. Note the increased interaction at MAM of Akt with its kinase mTORC2 and with its substrates IP3R and PACS2, suggesting that mTORC2 controls PACS2 and IP3R at MAM via Akt. Input in Fig. S5*B*. (*D*) Intracellular calcium release in MEFs after stimulation with 200 μM ATP, quantified by the emission ratio 340/380 nm after labeling with Fura2-AM. Data are normalized to the time point 0. $n = 104$. Cells were grown and labeled in normal medium before switching to calcium-free HBSS for the measurements. (*E*) Area under the curve (AUC) of *D*. (*F*) AUC of mitochondrial calcium uptake after stimulation with ATP. The cells were transiently transfected with the mitochondria-targeted Cameleon probe 4mtD3cpv and growing in normal medium before measurements. $n = 20$. (*G*) Original recording showing the ER Ca^{2+} depletion following TG treatment. For quantification, see *H*. (*H*) Statistical evaluation of the kinetic of ER calcium store depletion after addition of 1 μM TG, reflecting an increased ER Ca^{2+} leak in rictor KO MEFs. $n = 26$. The cells were transiently transfected with the ER-targeted Cameleon probe $D1_{ER}$. (*I*) AUC of intracellular calcium release after stimulation with 10 μM ionomycin in rictor KO and control MEFs, expressing LacZ or Akt S473D. Cells were labeled with Fura2-AM. Note that rictor KO MEFs have increased calcium stores. Cells were grown in normal medium before measurements. Results are shown as mean ± SEM and normalized to control cells. $^*P < 0.05$, $^{**}P < 0.01$, $^{***}P < 0.001$.

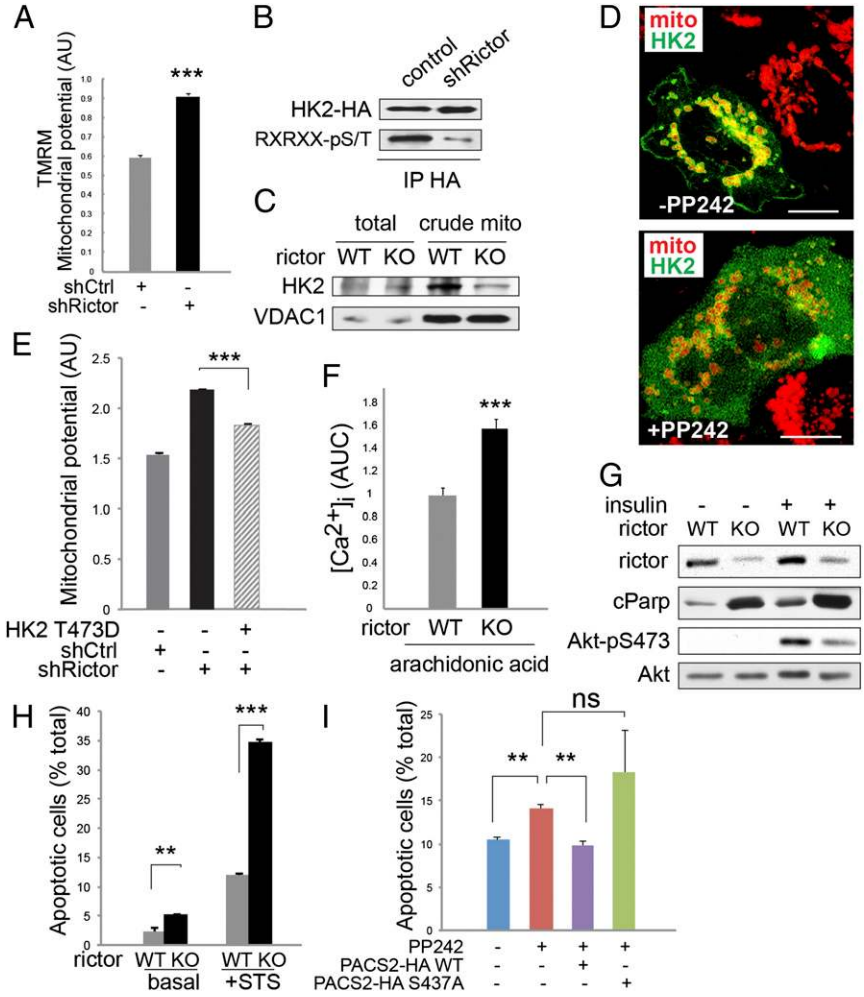

Fig. 5. mTORC2 at MAM controls mitochondrial function. (*A*) Mitochondrial potential of HeLa cells after rictor knockdown (shRictor), measured by TMRM intensity by FACS. Arbitrary units, $n = 3$. Cells were grown in normal medium before measurements. (*B*) Phosphorylation of HK2 by Akt is reduced in rictor knockdown cells. HK2-HA was immunoprecipitated and probed with a HA-tag or an Akt substrate motif antibody. Thirty-four hours after HK2 transfection, cells were serum-starved for 14 h, stimulated with insulin (100 nM) for 15 min, and lysed in RIPA buffer. (*C*) Crude mitochondrial HK2 levels are reduced in rictor KO MEFs. Cells were grown in normal medium before harvest. (*D*) Representative immunofluoresence picture of HeLa cells expressing mRFP-mito and GFP-HK2, showing cytoplasmic HK2 in presence of 500 nM mTOR inhibitor PP242. (Scale bar, 10 μm.) Cells were grown on slides and starved for 14 h, pre-treated with 500 nM PP242 or DMSO for 20 min and stimulated with 100 nM insulin for 15 min before fixation by PFA. (*E*) Mitochondrial potential (arbitrary units) as measured by TMRM of HeLa cells transfected with a plasmid overexpressing HK2 T473D, a phosphomimetic mutant of the Akt substrate site ($n = 3$). Cells were grown in normal medium. HK2 was transfected 48 h before measurement. (*F*) AUC of intracellular calcium release of MEFs after apoptotic stimulation with 80 μM arachidonic acid ($n = 67–70$). Cells were grown in normal medium. (*G*) Total protein lysates from MEFs after insulin stimulation, showing increased levels of cleaved Parp (cParp) in rictor KO MEFs. Cells were serum starved for 6 h and insulin-stimulated for 15 min before collection. (*H*) Apoptotic MEFs as determined by positive Annexin V staining, analyzed by FACS ($n = 3$). Cells were grown in normal medium and treated with staurosporine (0.5 μM, 30 min) where indicated. (*I*) Apoptotic HeLa (Annexin V^+) treated with 500 nm PP242 for 6 h ($n = 3$). Cells were transfected with plasmids expressing PACS2-WT or PACS2-S437A 48 h before experiment and grown in normal medium. Results are shown as mean ± SEM and normalized to control cells. $^{**}P < 0.01$, $^{***}P < 0.001$; ns, not significant.

measure MAM at higher resolution (8, 13, 59), we analyzed EM images of rictor KO livers (Fig. 3*C*). ER-mitochondrial contact sites were reduced ∼40% upon mTORC2 KO, although the total amounts of mitochondria and ER per cell were unchanged (Fig. 3*E*). Finally, as suggested by our above observation that insulin stimulates MAM localization of mTORC2, we found that insulin or refeeding stimulated MAM formation (Fig. S3 *B* and *F–H*) in an mTORC2-dependent manner (Fig. 3*F*). Thus, insulin signaling stimulates both localization of mTORC2 to MAM and mTORC2-dependent MAM integrity.

How does mTORC2 regulate MAM integrity? We investigated whether mTORC2 regulates MAM integrity via Akt-dependent phosphorylation of PACS2, as suggested by the observation that the Akt substrate PACS2 is required for MAM integrity (13, 17) and our previous finding that Akt1 KO affects MAM integrity (Fig. S3*E*). First, Akt-mediated PACS2 phosphorylation was reduced in rictor knockdown cells (Fig. 3 *G* and *H*) or in cells treated with an Akt kinase inhibitor (Fig. 3*I* and Fig. S3*J*). Second, PACS2 interaction with Akt at MAM was stimulated by insulin treatment (Fig. 4*C* and Fig. S5*B*). Third, overexpression of either constitutively active Akt (Akt-S473D) or wild-type PACS2 restored MAM integrity in cells in which mTOR was pharmacologically inhibited (Fig. S3*K*). Fourth, overexpression of wild-type PACS2, but not PACS2 mutated at its Akt phosphorylation site (PACS2-S437A), suppressed the defect in MAM integrity observed upon rictor knockdown (Fig. 3*J* and Fig. S3*I*). Thus, mTORC2 at MAM appears to control MAM integrity through Akt-dependent PACS2 phosphorylation.

mTORC2 Controls Calcium Flux. Does mTORC2-Akt signaling control other processes at MAM? We investigated whether mTORC2 at MAM also controls Akt-dependent IP3R phosphorylation and function (see below for Akt target HK2). There are three IP3R isoforms, all of which contain an Akt target site (26), but Akt inhibits ER calcium release mainly through IP3R3 (25). We thus examined the effect of mTORC2 deficiency on phosphorylation of the Akt site specifically in IP3R3. IP3R3 phosphorylation was strongly reduced in MEFs upon rictor KO (Fig. 4 *A* and *B*) and in HeLa cells in which mTOR was pharmacologically inhibited (Fig. S5*A*). Furthermore, the interaction between Akt and IP3R at MAM was stimulated by insulin (Fig. 4*C* and Fig. S5*B*) and inhibited by MAM disruption (Fig. S6 *B* and *C*). Although IP3R levels were not affected by mTORC2 disruption (Fig. 4*B* and Fig. S4 *A* and *B*), rictor KO slightly enhanced detection of IP3R by immunoprecipitation (Figs. 3*B* and 4*A*). Thus, we asked whether mTORC2 masks the epitope recognized by the IP3R antibody. Using IP conditions that disrupt mTORC2, we immunoprecipitated the same amount of IP3R3 from wild-type and rictor KO cells (Fig. S5 *C* and *D*), confirming that intact mTORC2 masks the IP3R epitope.

Because calcium flux between the ER and mitochondria via IP3R is one of the main functions of MAM (60), we investigated whether calcium flux was disturbed in rictor KO cells. In particular, we measured changes in cytosolic calcium concentration upon stimulation with ATP or thapsigargin (TG). Importantly, we used cells suspended in calcium-free medium to rule out an effect due to influx of extracellular calcium. Like MAM-deficient cells (8, 13, 15), rictor KO MEFs displayed an increase in intracellular calcium $[Ca^{2+}]_i$ upon either ATP or TG treatment (Fig. 4 *D* and *E*, and Fig. S5 *E*–*G*). Overexpression of constitutively active Akt (Akt-S473D) suppressed the enhanced TG-stimulated increase in $[Ca^{2+}]_i$ in mTORC2 KO cells (Fig. S5 *F* and *G*), consistent with the previous finding that active Akt inhibits IP3R-mediated calcium release (25). Thus, mTORC2-Akt regulates IP3R3 phosphorylation and calcium release at MAM.

A previous study reported that a defect in the MAM tethering factor Mfn2 causes an increase in calcium uptake by mitochondria (8). We examined whether a MAM deficiency caused by an mTORC2 defect elicits a similar effect. Indeed, rictor KO MEFs exhibited an increase in calcium uptake by mitochondria, as measured by a fluorescent mitochondrial calcium reporter protein (Fig. 4*F* and Fig. S5*H*). This finding further indicates that an mTORC2 deficiency causes a MAM defect. The above observations are counterintuitive because a reduction rather than an increase in calcium uptake by mitochondria might be expected in cells in which the ER-mitochondria synapse is disturbed. This seemingly paradoxical finding has been explained by the fact that MAM-deficient cells, possibly as a compensatory mechanism, contain larger ER calcium stores and thus release more calcium for uptake by mitochondria (8). Accordingly, we also observed increased ER calcium stores in both mTORC2-deficient and Akt1 KO cells (Fig. 4*I* and Fig. S5 *I*–*K*) and enhanced calcium release from the ER in mTORC2 KO cells (Fig. 4 *G* and *H*). These findings can explain the increased transfer of calcium from the ER to the mitochondria observed in mTORC2 (Fig. 4*F*) and MAM-deficient cells (8). We conclude that the enhanced calcium release in mTORC2-deficient cells is caused by defective mTORC2-Akt signaling at MAM. In particular, the enhanced calcium release is likely because of defects in mTORC2-Akt mediated IP3R phosphorylation and MAM integrity.

mTORC2 Controls Mitochondrial Physiology. Observations described above and elsewhere (see introductory paragraphs) suggest that mTORC2, like other regulators of MAM integrity (61), affects mitochondrial function. We therefore examined whether the mitochondrial inner membrane potential ($\Delta\Psi_m$), an important indicator of mitochondrial function, is regulated by mTORC2. mTORC2 and Akt-deficient cells exhibited an increase in $\Delta\Psi_m$ as measured by increased tetramethylrhodamine methyl ester (TMRM) fluorescence (Fig. 5*A* and Fig. S6 *F*–*J*) and ATP concentration (Fig. S6*M*). The detected increase in $\Delta\Psi_m$ was not caused by a change in mitochondrial content (Fig. S6*K*). These observations are consistent with the previous finding that rictor knockdown leads to an increase in mitochondrial respiration (62).

How does mTORC2 control $\Delta\Psi_m$? HK2 is mitochondria-associated and an Akt substrate (18, 19). Phosphorylation of HK2-T473 by Akt stabilizes HK2 binding to the MAM protein VDAC1. HK2 binding to VDAC1 stimulates glycolysis and inhibits $\Delta\Psi_m$ (see introductory paragraphs) (18, 19). We examined whether mTORC2 controls Akt-dependent HK2-T473 phosphorylation. HK2-T473 phosphorylation was reduced upon rictor knockdown or pharmacological inhibition of mTOR (Fig. 5*B* and Fig. S6*A*). Furthermore, insulin stimulated recruitment of HK2 to mitochondria, likely MAM, in an mTORC2-dependent manner (Fig. 5 *C* and *D*). HK2 interacted preferentially with activated Akt (Fig. S6 *D* and *E*), and the interaction between Akt and HK2 was reduced in MAM-deficient cells (Fig. S6 *B* and *C*). The increase in $\Delta\Psi_m$ in rictor KO cells was suppressed by overexpression of activated Akt (Akt-S473D) (Fig. S6*O*) or mutant HK2 containing a phosphomimetic residue at position 473 (HK2-T473D) (Fig. 5*E*). As expected, overexpression of HK2-T473A increased $\Delta\Psi_m$ in wild-type cells (Fig. S6*L*). Interestingly, overexpression of wild-type PACS2 did not suppress the enhanced $\Delta\Psi_m$ caused by mTORC2 inhibition (Fig. S6*I*), suggesting that the increase in $\Delta\Psi_m$ is independent of the defect in MAM integrity. Thus, mTORC2 at MAM controls mitochondrial physiology, at least in part, via Akt-mediated regulation of HK2.

Mitochondria play a pivotal role in apoptosis. Arachidonic acid induces apoptosis by stimulating the transfer of calcium from the ER to mitochondria at MAM (25). Calcium release was enhanced in rictor KO MEFs upon arachidonic acid treatment, compared with wild-type MEFs (Fig. 5*F*). Furthermore, an mTORC2 deficiency led to elevated levels of apoptosis (Fig. 5 *G* and *H*). As measured by Annexin V staining, pharmacologic inhibition of mTOR (Fig. 5*I*) or disruption of mTORC2 (Fig. S6*N*) also caused an increase in apoptosis that could be suppressed by overexpression of wild-type PACS2. These findings indicate that mTORC2 regulates apoptosis at least partly through PACS2 and MAM. Thus, mTORC2 at MAM appears to control several aspects of mitochondrial physiology (Fig. S7).

Discussion

We show that mTORC2 is physically associated with MAM, and that mTORC2-Akt signaling mediates MAM integrity and function. mTORC2 localizes to MAM in a growth factor-stimulated manner where it phosphorylates and activates Akt. Akt in turn phosphorylates the MAM resident proteins PACS2, IP3R, and HK2, to regulate MAM integrity, calcium flux, and energy metabolism, respectively. Accordingly, we find that mTORC2 disruption phenotypically mimics a MAM deficiency. Thus, MAM appears to be an mTORC2 signaling hub.

mTORC2 is activated by association with the ribosome (34). Here we report that mTORC2 is active at MAM. Is mTORC2 at MAM activated by ribosome association? We find that mTORC2 at MAM is indeed associated with ribosomes. EM studies (59, 63, 64) and proteomic profiling (20, 21, 65) of MAM suggest that ribosomes are present at this ER subdomain. Zhang et al. (20) reported an increase in the number of ribosomes at MAM after CMV infection, a virus that is known to activate mTORC2 (66). Finally, calnexin, a MAM-enriched chaperone (54), interacts with PACS2 and anchors ribosomes at the ER and possibly MAM (67). Although it remains to be determined whether calnexin is indeed involved in localization of ribosomes to MAM or in mTORC2 signaling, taken together, the above data suggest that mTORC2 at MAM is activated by ribosome association.

Akt is generally thought to be localized to the plasma membrane, upon binding of its pleckstrin homology domain to phosphatidylinositol(3,4,5)-trisphosphate, where it is phosphorylated by phosphoinositide-dependent protein kinase-1 at T308 and by mTORC2 at S473. However, previous studies have reported active Akt at mitochondria and MAM (16, 18, 48, 49). Furthermore, mTORC2 can phosphorylate Akt at the ER (39) and ER stress inhibits mTORC2 activity (42), suggesting functional mTORC2-Akt signaling at the ER/MAM. Thus, there appears to be spatially distinct mTORC2 signaling pathways. Interestingly, there are at least three different versions of mTORC2, each containing a distinct Sin1 isoform (68).

mTORC2 appears to regulate MAM integrity via phosphorylation of PACS2 at S437 by Akt, because overexpression of wild-type PACS2 but not PACS2-S437A suppresses the MAM integrity defect caused by mTORC2 disruption. If phosphorylation of PACS2 at S437 is indeed mediating MAM integrity, how does overexpression of wild-type PACS2 rescue MAM integrity, even though phosphorylation of PACS2 by Akt is strongly reduced in mTORC2 deficient cells (Fig. 3*F*)? We hypothesize that wild-type PACS2 can act as a multicopy suppressor, much like overexpression of SGK or Akt in worms can suppress the phenotype of a rictor KO (69).

We report that hepatocytes from liver-specific rictor KO mice are defective for MAM. Hagiwara et al. recently reported that liver-specific rictor KO mice have whole-body metabolic defects (70). Interestingly, liver-specific KO of Mfn2, a key MAM protein, confers a whole-body phenotype strikingly similar to that of liver-specific rictor KO (12). Both KO mice exhibit increased gluconeogenesis, hyperinsulinemia, and glucose intolerance. This strong metabolic phenotype is consistent with the fact that the liver relies heavily on MAM function and that MAM mediates glucose metabolism (20, 57). Furthermore, a previously reported whole-genome shRNA screen revealed that mTORC2-addicted cancer cells are dependent on mitochondrial function and in particular HK2 (51). Thus, MAM appears to be a particularly important hub for mTORC2 signaling in the control of growth and metabolism.

In summary, we demonstrate that mTORC2 can localize to MAM, where it controls growth factor-mediated MAM integrity, calcium flux, and mitochondrial physiology. mTORC2 controls these processes via Akt which regulates PACS2, IP3R, and HK2. The combined action of these substrates affects energy metabolism and cell survival. Although the role of MAM localized mTORC2 in disease remains to be clarified, it is tempting to speculate that there could be beneficial effects of novel therapeutic interventions that specifically target mTORC2 localized to MAM.

Materials and Methods

Cell Culture. HeLa and inducible rictor knock-out MEFs were cultured, transfected, stimulated, and harvested as described previously (35, 71, 72). Mfn1/2 KO and respective control MEFs were purchased from ATCC. For details see *SI Materials and Methods*.

Plasmids. GFP-tagged HK2 was kindly provided by Alenoush Vartanian (The Hospital for Sick Children, Arthur and Sonia Labatt Brain Tumor Research Centre, Toronto). HA-tagged mouse HK2 (HA-HK2) in pcDNA3.1 was kindly provided by Nobuyuki Tanaka (Department of Molecular Oncology, Graduate School of Medicine, Nippon Medical School, Tokyo) (73). HK2-T473D was generated from HA-HK2 by mutagenesis (74) using the following primers GAAGgacCTGGAGTCTCTGAAGC and CAGgtcCTTCTGGCGGGCCC. Mutagenesis was sequence verified. Adenoviral LacZ, Akt-WT and Akt-S473D were produced and used as previously described (70). PACS2-HA and PACS2-S437A-HA (17) were obtained from Gary Thomas (Vollum Institute, Oregon Health and Science University, Portland, OR); 4mtD3cpv was kindly provided by Amy Palmer (Department of Chemistry, BioFrontiers Institute, University of Colorado, Boulder, CO) and Roger Tsien (Department of Chemistry and Biochemistry, and Howard Hughes Medical Institute, University of California, San Diego, La Jolla, CA). PACS2-Flag was purchased from Origene.

Protein Lysates, Fractionation, and Immunoprecipitation. Protein extracts were prepared as described previously (35, 71), resolved on SDS/PAGE, and transferred to nitrocellulose membranes (Protran, Whatman). Immunoprecipitation and immunoblotting were performed as described previously (34, 35, 71). Equal amounts for protein from different subcellular fractions were compared by immunoblotting. For details, see *SI Materials and Methods*.

Mice. Mice were generated as previously described (70). All experiments were performed in accordance with federal guidelines and were approved by the Kantonales Veterinäramt of Kanton Basel-Stadt. For insulin stimulation, the mice were starved for 14–16 h overnight, then injected intraperitoneally with 4.5 mg/kg insulin or saline 30 min before being killed. Refed mice were starved for 14–16 h overnight, then refed a standard chow diet for 2 h.

Microscopy. For organelle fluorescence labeling, cells were infected 24 h before harvest with baculovirus expressing ER-GFP or Mito-RFP (BacMAM; Life Technologies). Cells were seeded on 12-mm glass slides 24 h before the experiment. For details, see *SI Materials and Methods*.

Statistical Analyses, Data are expressed as average ± SEM of at least three independent experiments. Unpaired *t* test was used to determine differences between two groups. Significance was judged when $P < 0.05$.

ACKNOWLEDGMENTS. We thank Asami Hagiwara, Marion Cornu, Cyril Castelbou, Estela Jacinto, and Don Benjamin for assistance or reagents. Immunofluorescent images were acquired at the Imaging Core Facility, Biozentrum Basel. This work was supported in part by the Leslie Misrock Foundation (C.B.), the Swiss National Science Foundation, SystemsX.ch, the Swiss Cancer League, the Louis Jeantet Foundation, and the Canton of Basel.

1. Csordás G, Thomas A, Hajnóczky G (1999) Quasi-synaptic calcium signal transmission between endoplasmic reticulum and mitochondria. *EMBO J* 18(1):96–108.
2. Rizzuto R, et al. (1998) Close contacts with the endoplasmic reticulum as determinants of mitochondrial Ca2+ responses. *Science* 280(5370):1763–1766.
3. Stone SJ, et al. (2009) The endoplasmic reticulum enzyme DGAT2 is found in mitochondria-associated membranes and has a mitochondrial targeting signal that promotes its association with mitochondria. *J Biol Chem* 284(8):5352–5361.
4. Ardail D, et al. (2003) The mitochondria-associated endoplasmic-reticulum subcompartment (MAM fraction) of rat liver contains highly active sphingolipid-specific glycosyltransferases. *Biochem J* 371(Pt 3):1013–1019.
5. Bionda C, Portoukalian J, Schmitt D, Rodriguez-Lafrasse C, Ardail D (2004) Subcellular compartmentalization of ceramide metabolism: MAM (mitochondria-associated membrane) and/or mitochondria? *Biochem J* 382(Pt 2):527–533.
6. Vance JE (1990) Phospholipid synthesis in a membrane fraction associated with mitochondria. *J Biol Chem* 265(13):7248–7256.
7. Szabadkai G, et al. (2006) Chaperone-mediated coupling of endoplasmic reticulum and mitochondrial Ca2+ channels. *J Cell Biol* 175(6):901–911.
8. de Brito OM, Scorrano L (2008) Mitofusin 2 tethers endoplasmic reticulum to mitochondria. *Nature* 456(7222):605–610.
9. Marriott K-SC, Prasad M, Thapliyal V, Bose HS (2012) σ-1 receptor at the mitochondrial-associated endoplasmic reticulum membrane is responsible for mitochondrial metabolic regulation. *J Pharmacol Exp Ther* 343(3):578–586.
10. Pizzo P, Pozzan T (2007) Mitochondria-endoplasmic reticulum choreography: Structure and signaling dynamics. *Trends Cell Biol* 17(10):511–517.
11. Pawlikowska P, Gajkowska B, Orzechowski A (2007) Mitofusin 2 (Mfn2): A key player in insulin-dependent myogenesis in vitro. *Cell Tissue Res* 327(3):571–581.
12. Sebastián D, et al. (2012) Mitofusin 2 (Mfn2) links mitochondrial and endoplasmic reticulum function with insulin signaling and is essential for normal glucose homeostasis. *Proc Natl Acad Sci USA* 109(14):5523–5528.
13. Simmen T, et al. (2005) PACS-2 controls endoplasmic reticulum-mitochondria communication and Bid-mediated apoptosis. *EMBO J* 24(4):717–729.
14. Myhill N, et al. (2008) The subcellular distribution of calnexin is mediated by PACS-2. *Mol Biol Cell* 19(7):2777–2788.
15. Bui M, et al. (2010) Rab32 modulates apoptosis onset and mitochondria-associated membrane (MAM) properties. *J Biol Chem* 285(41):31590–31602.
16. Giorgi C, et al. (2010) PML regulates apoptosis at endoplasmic reticulum by modulating calcium release. *Science* 330(6008):1247–1251.
17. Aslan JE, et al. (2009) Akt and 14-3-3 control a PACS-2 homeostatic switch that integrates membrane traffic with TRAIL-induced apoptosis. *Mol Cell* 34(4):497–509.
18. Miyamoto S, Murphy AN, Brown JH (2008) Akt mediates mitochondrial protection in cardiomyocytes through phosphorylation of mitochondrial hexokinase-II. *Cell Death Differ* 15(3):521–529.
19. Gottlob K, et al. (2001) Inhibition of early apoptotic events by Akt/PKB is dependent on the first committed step of glycolysis and mitochondrial hexokinase. *Genes Dev* 15(11):1406–1418.

20. Zhang A, et al. (2011) Quantitative proteomic analyses of human cytomegalovirus-induced restructuring of endoplasmic reticulum-mitochondrial contacts at late times of infection. *Mol Cell Proteomics* 10(10):M111. 009936.
21. Poston CN, Krishnan SC, Bazemore-Walker CR (2013) In-depth proteomic analysis of mammalian mitochondria-associated membranes (MAM). *J Proteomics* 79:219–230.
22. Stiles BL (2009) PI-3-K and AKT: Onto the mitochondria. *Adv Drug Deliv Rev* 61(14): 1276–1282.
23. Wolf A, et al. (2011) Hexokinase 2 is a key mediator of aerobic glycolysis and promotes tumor growth in human glioblastoma multiforme. *J Exp Med* 208(2):313–326.
24. Szado T, et al. (2008) Phosphorylation of inositol 1,4,5-trisphosphate receptors by protein kinase B/Akt inhibits Ca2+ release and apoptosis. *Proc Natl Acad Sci USA* 105 (7):2427–2432.
25. Marchi S, et al. (2012) Selective modulation of subtype III IP_3R by Akt regulates ER Ca^{2+} release and apoptosis. *Cell Death Dis* 3:e304.
26. Khan MT, Wagner L, 2nd, Yule DI, Bhanumathy C, Joseph SK (2006) Akt kinase phosphorylation of inositol 1,4,5-trisphosphate receptors. *J Biol Chem* 281(6): 3731–3737.
27. Raturi A, Simmen T (2013) Where the endoplasmic reticulum and the mitochondrion tie the knot: The mitochondria-associated membrane (MAM). *Biochim Biophys Acta* 1833(1):213–224.
28. Soulard A, Cohen A, Hall MN (2009) TOR signaling in invertebrates. *Curr Opin Cell Biol* 21(6):825–836.
29. Laplante M, Sabatini DM (2009) mTOR signaling at a glance. *J Cell Sci* 122(Pt 20): 3589–3594.
30. Wullschleger S, Loewith R, Hall MN (2006) TOR signaling in growth and metabolism. *Cell* 124(3):471–484.
31. Cybulski N, Hall MN (2009) TOR complex 2: A signaling pathway of its own. *Trends Biochem Sci* 34(12):620–627.
32. Oh WJ, Jacinto E (2011) mTOR complex 2 signaling and functions. *Cell Cycle* 10(14): 2305–2316.
33. Oh WJ, et al. (2010) mTORC2 can associate with ribosomes to promote cotranslational phosphorylation and stability of nascent Akt polypeptide. *EMBO J* 29(23):3939–3951.
34. Zinzalla V, Stracka D, Oppliger W, Hall MN (2011) Activation of mTORC2 by association with the ribosome. *Cell* 144(5):757–768.
35. Thedieck K, et al. (2007) PRAS40 and PRR5-like protein are new mTOR interactors that regulate apoptosis. *PLoS ONE* 2(11):e1217.
36. Sarbassov DD, Guertin DA, Ali SM, Sabatini DM (2005) Phosphorylation and regulation of Akt/PKB by the rictor-mTOR complex. *Science* 307(5712):1098–1101.
37. Yang Q, Inoki K, Ikenoue T, Guan K-L (2006) Identification of Sin1 as an essential TORC2 component required for complex formation and kinase activity. *Genes Dev* 20 (20):2820–2832.
38. Zhao L, Yue P, Khuri FR, Sun SY (2013) mTOR complex 2 is involved in regulation of Cbl-dependent c-FLIP degradation and sensitivity of TRAIL-induced apoptosis. *Cancer Res* 73(6):1946–1957.
39. Boulbés DR, Shaiken T, Sarbassov D (2011) Endoplasmic reticulum is a main localization site of mTORC2. *Biochem Biophys Res Commun* 413(1):46–52.
40. Hresko RC, Mueckler M (2005) mTOR.RICTOR is the Ser473 kinase for Akt/protein kinase B in 3T3-L1 adipocytes. *J Biol Chem* 280(49):40406–40416.
41. Chen CH, et al. (2011) ER stress inhibits mTORC2 and Akt signaling through GSK-3β-mediated phosphorylation of rictor. *Sci Signal* 4(161):ra10.
42. Appenzeller-Herzog C, Hall MN (2012) Bidirectional crosstalk between endoplasmic reticulum stress and mTOR signaling. *Trends Cell Biol* 22(5):274–282.
43. Díaz-Troya S, Florencio FJ, Crespo JL (2008) Target of rapamycin and LST8 proteins associate with membranes from the endoplasmic reticulum in the unicellular green alga *Chlamydomonas reinhardtii*. *Eukaryot Cell* 7(2):212–222.
44. Desai BN, Myers BR, Schreiber SL (2002) FKBP12-rapamycin-associated protein associates with mitochondria and senses osmotic stress via mitochondrial dysfunction. *Proc Natl Acad Sci USA* 99(7):4319–4324.
45. Ramanathan A, Schreiber SL (2009) Direct control of mitochondrial function by mTOR. *Proc Natl Acad Sci USA* 106(52):22229–22232.
46. Behrends C, Sowa ME, Gygi SP, Harper JW (2010) Network organization of the human autophagy system. *Nature* 466(7302):68–76.
47. Wang Y, Weiss LM, Orlofsky A (2010) Coordinate control of host centrosome position, organelle distribution, and migratory response by *Toxoplasma gondii* via host mTORC2. *J Biol Chem* 285(20):15611–15618.
48. Antico Arciuch VG, et al. (2009) Akt1 intramitochondrial cycling is a crucial step in the redox modulation of cell cycle progression. *PLoS ONE* 4(10):e7523.
49. Bijur GN, Jope RS (2003) Rapid accumulation of Akt in mitochondria following phosphatidylinositol 3-kinase activation. *J Neurochem* 87(6):1427–1435.
50. Murata H, et al. (2011) A new cytosolic pathway from a Parkinson disease-associated kinase, BRPK/PINK1: Activation of AKT via mTORC2. *J Biol Chem* 286(9):7182–7189.
51. Colombi M, et al. (2011) Genome-wide shRNA screen reveals increased mitochondrial dependence upon mTORC2 addiction. *Oncogene* 30(13):1551–1565.
52. Barquilla A, Crespo JL, Navarro M (2008) Rapamycin inhibits trypanosome cell growth by preventing TOR complex 2 formation. *Proc Natl Acad Sci USA* 105(38): 14579–14584.
53. Stephens SB, Dodd RD, Lerner RS, Pyhtila BM, Nicchitta CV (2008) Analysis of mRNA partitioning between the cytosol and endoplasmic reticulum compartments of mammalian cells. *Methods Mol Biol* 419:197–214.
54. Lynes EM, et al. (2012) Palmitoylated TMX and calnexin target to the mitochondria-associated membrane. *EMBO J* 31(2):457–470.
55. Horner SM, Liu HM, Park HS, Briley J, Gale M, Jr. (2011) Mitochondrial-associated endoplasmic reticulum membranes (MAM) form innate immune synapses and are targeted by hepatitis C virus. *Proc Natl Acad Sci USA* 108(35):14590–14595.
56. Wieckowski MR, Giorgi C, Lebiedzinska M, Duszynski J, Pinton P (2009) Isolation of mitochondria-associated membranes and mitochondria from animal tissues and cells. *Nat Protoc* 4(11):1582–1590.
57. Rusiñol AE, Cui Z, Chen MH, Vance JE (1994) A unique mitochondria-associated membrane fraction from rat liver has a high capacity for lipid synthesis and contains pre-Golgi secretory proteins including nascent lipoproteins. *J Biol Chem* 269(44): 27494–27502.
58. Adelman MR, Sabatini DD, Blobel G (1973) Ribosome-membrane interaction. Nondestructive disassembly of rat liver rough microsomes into ribosomal and membranous components. *J Cell Biol* 56(1):206–229.
59. Csordás G, et al. (2006) Structural and functional features and significance of the physical linkage between ER and mitochondria. *J Cell Biol* 174(7):915–921.
60. Bononi A, et al. (2012) Mitochondria-associated membranes (MAMs) as hotspot Ca(2+) signaling units. *Adv Exp Med Biol* 740:411–437.
61. de Brito OM, Scorrano L (2010) An intimate liaison: Spatial organization of the endoplasmic reticulum-mitochondria relationship. *EMBO J* 29(16):2715–2723.
62. Schieke SM, et al. (2006) The mammalian target of rapamycin (mTOR) pathway regulates mitochondrial oxygen consumption and oxidative capacity. *J Biol Chem* 281(37):27643–27652.
63. Lebiedzinska M, Szabadkai G, Jones AWE, Duszynski J, Wieckowski MR (2009) Interactions between the endoplasmic reticulum, mitochondria, plasma membrane and other subcellular organelles. *Int J Biochem Cell Biol* 41(10):1805–1816.
64. Ruby JR, Dyer RF, Skalko RG (1969) Continuities between mitochondria and endoplasmic reticulum in the mammalian ovary. *Z Zellforsch Mikrosk Anat* 97(1):30–37.
65. Poston CN, Duong E, Cao Y, Bazemore-Walker CR (2011) Proteomic analysis of lipid raft-enriched membranes isolated from internal organelles. *Biochem Biophys Res Commun* 415(2):355–360.
66. Clippinger AJ, Maguire TG, Alwine JC (2011) The changing role of mTOR kinase in the maintenance of protein synthesis during human cytomegalovirus infection. *J Virol* 85(8):3930–3939.
67. Lakkaraju AK, et al. (2012) Palmitoylated calnexin is a key component of the ribosome-translocon complex. *EMBO J* 31(7):1823–1835.
68. Frias MA, et al. (2006) mSin1 is necessary for Akt/PKB phosphorylation, and its isoforms define three distinct mTORC2s. *Curr Biol* 16(18):1865–1870.
69. Soukas AA, Kane EA, Carr CE, Melo JA, Ruvkun G (2009) Rictor/TORC2 regulates fat metabolism, feeding, growth, and life span in *Caenorhabditis elegans*. *Genes Dev* 23(4):496–511.
70. Hagiwara A, et al. (2012) Hepatic mTORC2 activates glycolysis and lipogenesis through Akt, Glucokinase, and SREBP1c. *Cell Metab* 15(5):725–738.
71. Jacinto E, et al. (2004) Mammalian TOR complex 2 controls the actin cytoskeleton and is rapamycin insensitive. *Nat Cell Biol* 6(11):1122–1128.
72. Cybulski N, Zinzalla V, Hall MN (2012) Inducible raptor and rictor knockout mouse embryonic fibroblasts. *Methods Mol Biol* 821:267–278.
73. Ando M, et al. (2010) Interleukin 6 enhances glycolysis through expression of the glycolytic enzymes hexokinase 2 and 6-phosphofructo-2-kinase/fructose-2, 6-bisphosphatase-3. *J Nippon Med Sch* 77(2):97–105.
74. Zheng L, Baumann U, Reymond J-L (2004) An efficient one-step site-directed and site-saturation mutagenesis protocol. *Nucleic Acids Res* 32(14):e115.

Supporting Information

Betz et al. 10.1073/pnas.1302455110

SI Materials and Methods

Cell Culture. Cells were seeded and grown for 48 h in DMEM supplemented with 10% (vol/vol) serum (basal conditions). Cells were starved of serum for 14 h unless noted otherwise before restimulation with 100 nM insulin (Sigma) for 15 min. Primary hepatocytes were isolated as previously described (6). For mTORC2 knockdown, HeLa cells were infected with lentiviruses carrying shControl or shRictor (TRC library; Sigma Aldrich) at a multiplicity of infection of 0.1. Cells were selected after 24 h with 1 μg/mL puromycin for 1 wk, then subcloned and kept under puromycin selection. Transfection was performed using X-tremegene HD (Roche) using 1 mL Optimem (Gibco), 6 μg plasmid DNA, and 18 μL transfection reagent per 10-cm dish. Transient siRNA-mediated knockdown was performed as described previously (7).

Protein Lysates, Fractionation, and Immunoprecipitation. Films were scanned on CanoScan 9000F and signals were quantified using densitometry functions of the FIJI application. For subfractionation, endoplasmic reticulum (ER) was isolated by isopycnic flotation using a previously described protocol (8). Preparation of crude and pure mitochondrial extracts and mitochondria-associated ER membrane (MAM) isolation were performed as previously published (9). Ribosome stripping was performed as previously published (10). Immunoprecipitation and mammalian target of rapamycin complex 2 (mTORC2) kinase assay was performed using a previously described protocol (11). Briefly, cells were lysed on the culture plates after one washing step with cold PBS. Lysates were precleared with respective protein A or G Sepharose beads for 20 min. Lysis buffer was either CHAPS IP buffer (0.3% CHAPS, 40 mM Hepes pH7.5, 120 mM NaCl, 1 mM EDTA, 10 mM pyrophosphate, 10 mM glyerophosphate, HALT phosphatase, and protease inhibitor; Promega) or RIPA buffer (1% Triton-X, 0.1% SDS, 0.5% deoxycholate, 50 mM Tris pH 7.5, 150 mM NaCl, HALT phosphatase, and protease inhibitor; Promega), as noted, respectively. Control/mock IP was performed using equal amount of mouse/rabbit or goat IgG, respectively. mTOR complex IPs were performed for 4 h with IP antibody, followed by 1 h in the presence of protein A Sepharose beads, both steps at 4 °C. Beads were washed three times in IP buffer, and loading buffer was added. IPs targeting the IP_3 receptor (IP3R) were boiled at 65 °C for 25 min instead of standard 95 °C for 5 min to prevent precipitation of the transmembrane proteins. To measure the phosphorylation status of IP3R, HeLa cells were starved for 14 h, treated with 500 nM PP242 or DMSO for 20 min and stimulated with 20% (vol/vol) FCS for 20 min. IP3R was immunoprecipitated and blots were probed with anti-IP3R or antiphospho-Akt-Substrate antibody. To measure the phosphorylation status of HK2, HeLa cells were transfected with HK2-HA 48 h before the experiment. HeLa cells were starved for 14 h, treated with 500 nM PP242 or DMSO for 20 min, and stimulated with 20% (vol/vol) FCS for 20 min. Blots were probed with anti-HA or antiphospho-Akt-Substrate antibody.

Microscopy. Cells were washed in PBS, fixed with 37 °C 4% (vol/vol) paraformaldehyde for 2 min, washed in PBS twice, treated with 0.1% TritonX 100 for 10 min at room temperature, and blocked in 3% (wt/vol) BSA for 1 h at room temperature. For immunofluorescence, primary antibodies were added over night at 4 °C (1:50 for anti-rictor, 1:200 for anti-HSP47), washed three times in PBS at room temperature, and incubated with secondary antibodies (anti-rabbit Alexa647 1:200, anti-mouse Alexa488 1:200) for 2 h at room temperature. Slides were washed three times in PBS and mounted in Mowiol mounting medium [2.4 g Mowiol 4-88; Calbiochem; 6 g glycerol, 6 mL water, 12 mL 0.2 M Trix pH8.5, 2.5% (wt/vol) (1,4,-diazobicycli-[2.2.2]-octane); Sigma-Aldrich]. Fluorescence was measured on LSM510 or LSM710. Images analyzing rictor localization or ER/mitochondrial colocalization were acquired using 3D-deconvoluted stacks using the Huygens application. Colocalization (Pearson's correlation coefficient) was measured with Imaris application using automatic thresholding.

For electron microscopy, mouse liver was cut into small pieces of 1–2 mm and fixed with 0.1 M phosphate buffer containing 3% (wt/vol) formaldehyde and 0.3% glutaraldehyde for 30 min at room temperature and with fresh fixative overnight at 4 °C. Then samples were washed with PBS three times for 30 min. Dehydratation was done at 4 °C in 50%, 70%, 90% (vol/vol) methanol/PBS each for 1 h. Infiltration with LR gold was done according to the manufacturer's instructions (LR gold, London Resin). Polymerization was done at –10 °C for 24 h. Sections of 75 nm were collected on Formvar/carbon-coated Ni-grids. Sections were stained for 15 min with 4% (wt/vol) uranyl-acetate and contrasted with lead-citrate for 60 s, visualized by a Philips EM100 electron microscope. Images were cropped for individual hepatocytes using Adobe Photoshop. Cell parameters, including ER length and mitochondrial size, were calculated using FIJI application.

Chemicals. Antibodies: mTOR, Akt, Akt pS473, Akt pT308, S6, PDI, insulin receptor, Lamp1, rictor IB, voltage-dependent anion-selective channel 1 (VDAC1), IP3R (=pan IP3R antibody), Grp75, phosphoinositide-dependent protein kinase-1, Rheb, HA, mitofusin 2 (Mfn2), RXRXXpS/T (9611), Hexokinase 2 (HK2), CoxI, cleaved Parp from Cell Signaling; Sin1, raptor, Rpl26 from Bethyl; PGK1, acyl CoA synthetase 4 (ACSL4), IP3R3 from Santa Cruz; phosphatidyl ethanolamine methyltransferase (PEMT2), rictor IF from Protein Atlas; Rab32 from Sigma; calnexin from BD Bioscience; CoxIV from Invitrogen; Hsp47 from Enzo Life Science; rictor EM from Abcam (ab104838); Rab5 antibody was obtained from Martin Spiess; rictor IP antibody was obtained from Markus Rüegg. Chemicals used were PP242 (Chemdea); insulin, ionomycin, thapsigargin and arachidonic acid (Sigma); Fura2-AM (Invitrogen).

Metabolic Measurements. Mitochondrial potential measurements were performed using MitoPT-TMRM (tetramethylrhodamine, methyl ester; ImmunoChemistry Technologies) following the manufacturers' instructions on a Bio-Rad Biomek NK; statistical analysis was performed using FlowJo 9.4. For mitochondrial Ca^{2+} measurements, mouse embryonic fibroblasts (MEFs) were transiently transfected with the ratiometric cameleon probe 4mtD3cpv targeted to the mitochondrial matrix 48 h before the experiments. Ratiometric images of Ca^{2+} signals were obtained using a microscope (Axio Observer, Zeiss) equipped with a Lambda DG4 illumination system (Sutter Instrument). Cells were illuminated at 440 nm (440AF21; Omega Optical) through a 455DRLP dichroic mirror, and emission was collected alternatively at 480 nm (480BP10; Omega Optical) and 535 nm (535AF26; Omega Optical), using a cooled, 12-bit CCD camera (CoolSnap HQ; Ropper Scientific). Image acquisition and analysis were performed with the Metafluor 6.3 software (Universal Imaging). Experiments were performed at room temperature in Hepes-buffered solution containing: 135 mM NaCl, 5 mM KCl, 1 mM $MgCl_2$, 1 mM EGTA, 10 Hepes, 10 mM glucose,

pH-adjusted at 7.45 with NaOH. For intracellular Ca^{2+} measurements, cells were plated 48 h before experiment on Lab-Tek chamber slides (ThermoFisher). Chambers were washed loaded for 30 min with HBSS plus calcium, 10% (vol/vol) FCS, and 1 μM Fura2-AM (Invitrogen). Ten minutes before measurement, the medium was replaced by adding calcium-free HBSS (Sigma) and the Fura2 signal was measured as described previously (12). The signal was captured and processed on Zeiss Cell Observer light microscope. Area under the curve (AUC) was calculated with Graphpad Prism 5 using baseline correction. Stimulations were performed with 200 μM ATP, 10 μM thapsigargin (TG), 80 μM arachidonic acid, or 10 μM ionomycin. For apoptosis measurements, Annexin V Alexa Fluor 488 (Invitrogen) measurements were performed as previously described (13). ATP was quantified using CellTiter-Glo Luminescent assay (Promega).

Statistics. Student's *t* test was calculated using QuickTTestX 1.0 application.

1. Yang Q, Inoki K, Ikenoue T, Guan K-L (2006) Identification of Sin1 as an essential TORC2 component required for complex formation and kinase activity. *Genes Dev* 20(20):2820–2832.
2. Frias MA, et al. (2006) mSin1 is necessary for Akt/PKB phosphorylation, and its isoforms define three distinct mTORC2s. *Curr Biol* 16(18):1865–1870.
3. Kim SJ, et al. (2012) mTOR complex 2 regulates proper turnover of insulin receptor substrate-1 via the ubiquitin ligase subunit Fbw8. *Mol Cell* 48(6):875–887.
4. Thedieck K, et al. (2007) PRAS40 and PRR5-like protein are new mTOR interactors that regulate apoptosis. *PLoS ONE* 2(11):e1217.
5. Treins C, Warne PH, Magnuson MA, Pende M, Downward J (2010) Rictor is a novel target of p70 S6 kinase-1. *Oncogene* 29(7):1003–1016.
6. Hagiwara A, et al. (2012) Hepatic mTORC2 activates glycolysis and lipogenesis through Akt, Glucokinase, and SREBP1c. *Cell Metab* 15(5):725–738.
7. Durán RV, et al. (2012) Glutaminolysis activates Rag-mTORC1 signaling. *Mol Cell* 47(3): 349–358.
8. Stephens SB, Dodd RD, Lerner RS, Pyhtila BM, Nicchitta CV (2008) Analysis of mRNA partitioning between the cytosol and endoplasmic reticulum compartments of mammalian cells. *Methods Mol Biol* 419:197–214.
9. Wieckowski MR, Giorgi C, Lebiedzinska M, Duszynski J, Pinton P (2009) Isolation of mitochondria-associated membranes and mitochondria from animal tissues and cells. *Nat Protoc* 4(11):1582–1590.
10. Adelman MR, Sabatini DD, Blobel G (1973) Ribosome-membrane interaction. Nondestructive disassembly of rat liver rough microsomes into ribosomal and membranous components. *J Cell Biol* 56(1):206–229.
11. Zinzalla V, Stracka D, Oppliger W, Hall MN (2011) Activation of mTORC2 by association with the ribosome. *Cell* 144(5):757–768.
12. de Brito OM, Scorrano L (2008) Mitofusin 2 tethers endoplasmic reticulum to mitochondria. *Nature* 456(7222):605–610.
13. Colombi M, et al. (2011) Genome-wide shRNA screen reveals increased mitochondrial dependence upon mTORC2 addiction. *Oncogene* 30(13):1551–1565.

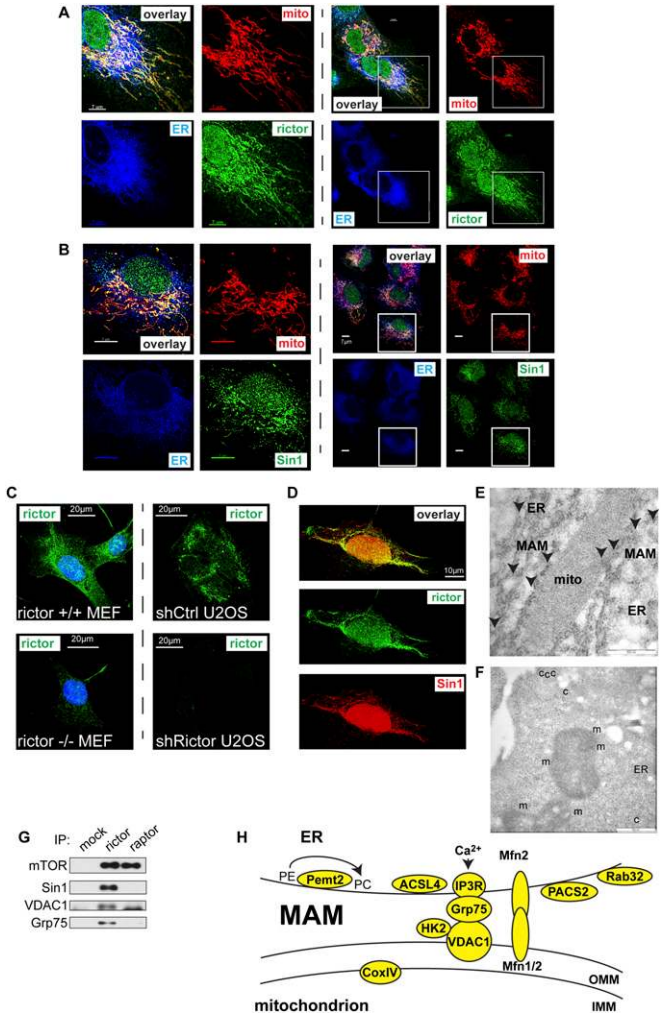

Fig. S1. (*A*) Individual channels from Fig. 1*C*, showing ER (blue, ER-GFP, BACMAM 2; Invitrogen), mitochondria (red, Mito-RFP, BACMAM 2; Invitrogen), and endogenous rictor (green) in U2OS cells. (Scale bar, 7 μm.) Shown is maximum-intensity projection of 3D-deconvoluted, confocal image stack. (*Left*) Zoomed-in view from *Right*. (*B*) Immunofluorescent image showing ER (blue, ER-GFP), mitochondria (red, Mito-RFP), and endogenous Sin1 (green) in U2OS cells. (Scale bar, 7 μm.) Cells were grown on coverslips in normal medium before PFA fixation. (*C*) Control for specificity of the rictor antibody. Rictor was stained as previously in inducible rictor KO and control MEFs (*Left*, counterstained with DAPI) or in U2OS cells with a stable rictor knockdown (*Right*). Acquisition settings for image pairs are equal. (Scale bar, 20 μm.) Cells were grown on coverslips in normal medium before PFA fixation. (*D*) Immunofluorescent image showing overlap of endogenous rictor (green) and endogenous Sin1 (red) in U2OS cells. (Scale bar, 10 μm.) Cells were grown on coverslips in normal medium before PFA fixation. (*E*) Electron micrograph of wild-type mouse liver slices staining for rictor (arrowheads). Mito, mitochondrion. (Scale bar, 500 nm.) Mice were fed a standard chow diet and killed in the morning. (*F*) Electron micrograph of HEK293T cells staining for rictor; m, rictor in proximity to mitochondrion; c, rictor in cytosol or attached to unidentified organelle. (Scale bar, 500 nm.) Cells were grown in normal medium before fixation. Unlike in liver cells, the ER is not clearly visible in HEK cells. Forty-eight percent of rictor was cytosolic, 38% associated with mitochondria, 11% in close proximity with the plasma membrane, and 4% was nuclear ($n = 7$). (*G*) mTORC2 (rictor) but not mTORC1 (raptor) coimmunoprecipitates the MAM tether VDAC1-Grp75. Mouse liver extracts were used as starting material for IP. Lower band in VDAC1 panel represents signal from light antibody chain. (*H*) Schematic overview of MAM including marker proteins used in this study.

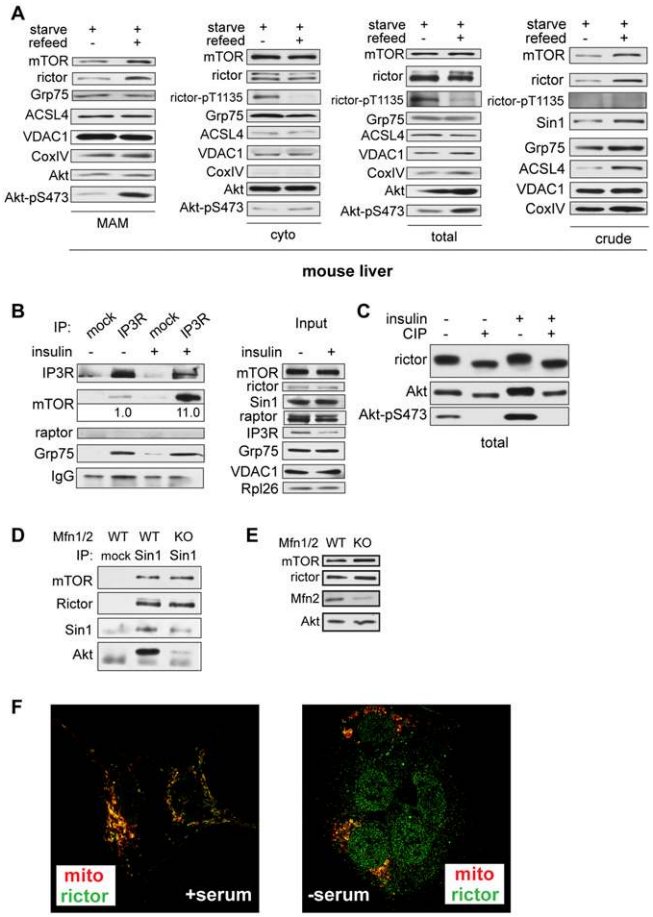

Fig. S2. (*A*) mTORC2 localization to MAM is increased in livers of refed control mice, indicating that increased mTORC2 localization to MAM is also observed under physiological stimulation by food intake. Mice were starved for 14 h and refed standard diet for 2 h. Shown are MAM, cytoplasmic, crude mitochondrial and total extracts. Rictor-pT1135 was not detected in MAM fraction and is thus not shown. Equal amount of total proteins are loaded in each lane. (*B*, *Left*) mTORC2-IP3R-Grp75 interaction is increased in total liver extracts from mice that were starved for 14 h and injected intraperitoneally with 4.5 mg/kg insulin or saline 30 min before being killed. Proteins were quantified relative to starved state. (*Right*) Total protein levels for Fig. 2*D* and panel *B*. (*C*) Rictor is hyperphosphorylated. Total proteins were extracted from mouse livers of mice that were starved for 14 h and injected intraperitoneally with 4.5 mg/kg insulin or saline 30 min before being killed. Lysates were treated with calf intestinal phosphatase (CIP; New England Biolabs) following the manufacturer's instructions. Note the band shift upon CIP treatment in rictor and Akt. (*D*) Immunoprecipitation of mTORC2 from total lysates of control and MAM-deficient Mfn1/2 KO MEFs. Cells were growing in normal medium before harvest and IP was performed as done previously in CHAPS IP buffer. Note that mTORC2 substrate Akt binding to mTORC2 is reduced in MAM-deficient cells, indicating that MAM is a major site of mTORC2 activity. (*E*) Total lysates of control and MAM-deficient Mfn1/2 KO MEFs. (*F*) Colocalization of rictor (green) and mitochondria (mito-RFP, red, BACMAM 2; Invitrogen), showing a diffuse localization for endogenous rictor (nucleus) upon serum starvation in U2OS cells. Quantification shown in Fig. 2*E*. Cells were growing on coverslips in presence or absence (14 h) of serum before fixation. (Magnification: *F*, 630×.)

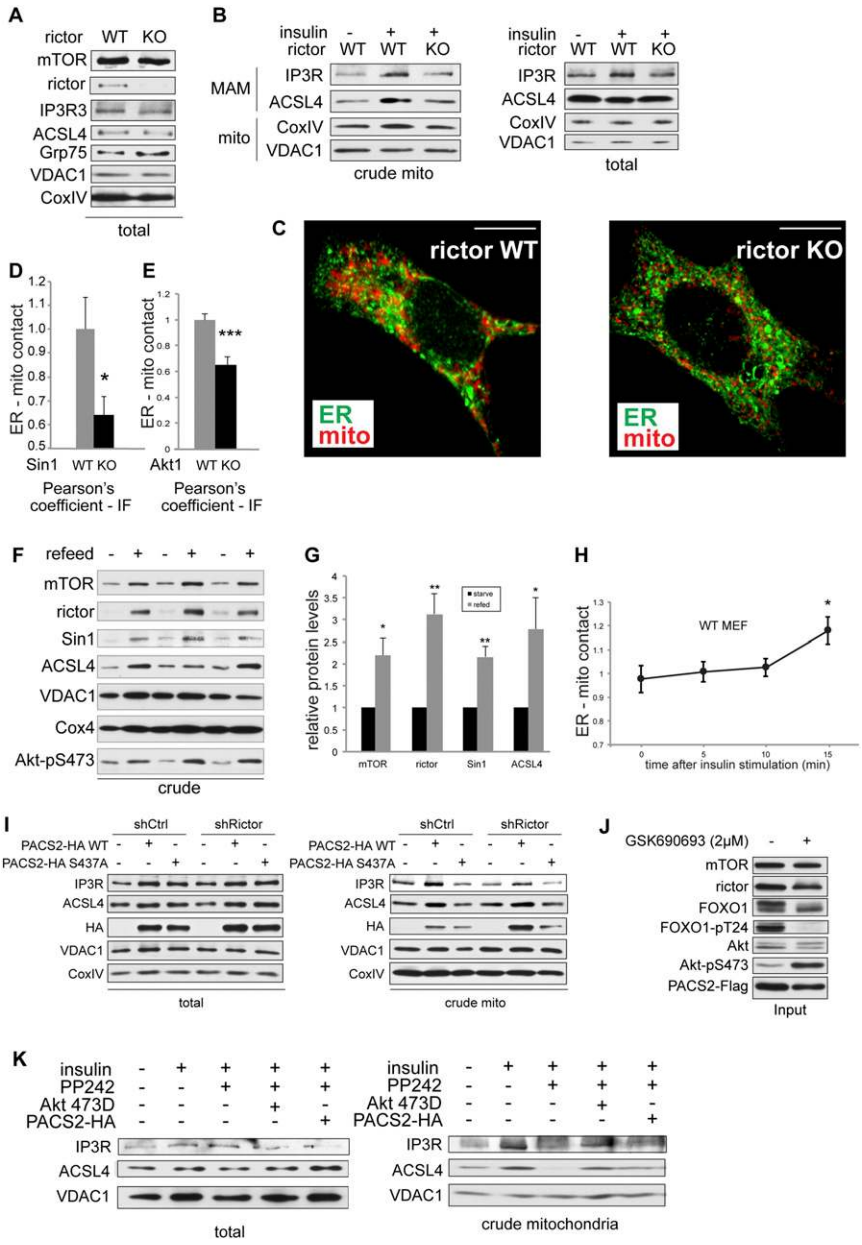

Fig. S3. (*A*) Total lysate fraction from Fig. 3*A*. (*B*) Total and crude mitochondrial extracts from livers of rictor KO or control littermate mice that were starved for 14 h and injected intraperitoneally with 4.5 mg/kg insulin or saline 30 min before being killed, showing mTORC2-dependent, insulin-stimulated accumulation of MAM marker proteins IP3R and ACSL4 in crude mitochondrial extracts. (*C*) Maximum intensity proection of representative confocal image stacks of rictor KO MEFs and control cells used for quantification of MAM in Fig. 3*D*. Cells expressed ER-GFP and mito-RFP (BACMAM 2; Invitrogen). (Scale bar, 10 μm.) (*D*) Pearson's correlation coefficient quantifying ER-mitochondrial contact as previously of Sin1 KO MEFs compared with their respective control cell line. Correlation coefficient was normalized to control cells ($n = 4$–5). (*E*) Pearson's correlation coefficient quantifying ER-mitochondrial contact as previously of Akt1 KO MEFs compared with their respective control cell line. (*F*) Crude mitochondrial extract of mouse liver cells. For corresponding MAM extracts, see Fig. 2*B*. Mice were starved for 14 h and refed for 2 h before being killed. Quantified in *G*. Extracts from two mice were pooled for each purification. (*G*) Densitometric quantification of protein levels in crude mitochondrial fraction from *F*. Note that unlike for MAM extracts (Fig. 2*B*), crude mitochondrial extracts show an increase in MAM markers when normalized to the mitochondrial VDAC1. (*H*) Life cell quantification time course of MAM in a control MEF cell line showing increased MAM formation 15 min after a 100 nM insulin stimulation relative to the starved state. Significance is calculated relative to $t = 0$ after the insulin stimulation, $n = 7$. (*I*) Total and crude mitochondrial extracts of HeLa cells after control (shCtrl) or mTORC2 knockdown (shRictor). Cells were transfected with phosphofurin acidic cluster sorting protein 2 (PACS2)-WT or PACS2-S473A 48 h before harvest and grown in normal medium. (*J*) Input of *I*. Note that even though the inhibitor induces hyperphosphorylation of Akt-pS473, Akt activity is inhibited, as judged by absence of FOXO1 phosphorylation. (*K*) Total and crude mitochondrial extracts of HeLa cells that were serum-starved for 14 h and treated with insulin 100 nM 15 min, mTOR inhibitor PP242 (500 nM, 10 min pretreatment and 15 min treatment during insulin stimulation). Cells overexpressed either Akt-S473D or PACS2 where indicated. Note the increase of MAM markers in the crude mitochondrial fraction upon insulin stimulation that is blocked by PP242. Results are shown as mean ± SEM and normalized to wild-type cells. $*P < 0.05$, $**P < 0.01$, $***P < 0.001$.

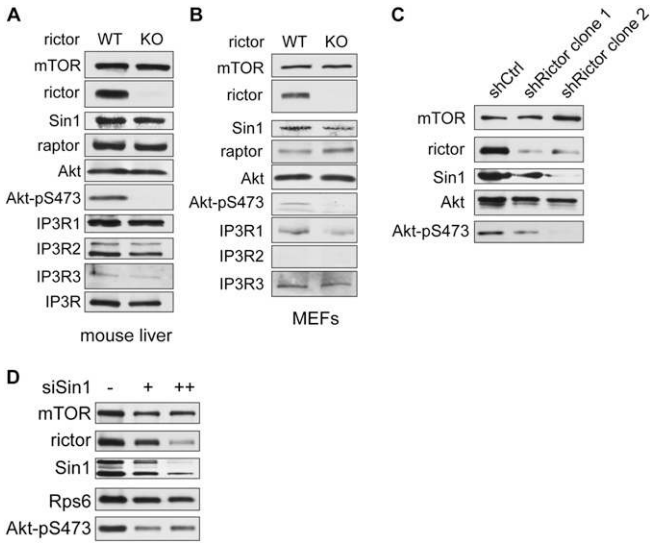

Fig. S4. (*A*) Total protein extracts from livers of a liver specific rictor KO and a control mouse showing rictor KO and reduced mTORC2 activity but no reduction in the IP3R isoforms. Note that Sin1 levels are not affected by genetic KO of rictor. Mice were starved for 14 h and injected intraperitoneally with 4.5 mg/kg insulin or saline 30 min before being killed. (*B*) Total protein extracts from MEFs where rictor KO had been induced by tamoxifen treatment and their respective controls, showing rictor KO and reduced mTORC2 activity but no reduction in the IP3R isoforms or Sin1. Cells were growing in normal medium before harvest. (*C*) Total protein extracts from stable rictor knockdown (shRictor) HeLa cells, showing reduction of Sin1 levels as previously reported (1–5). Cells were grown in normal medium and stimulated with 100 nM insulin for 15 min before harvest. (*D*) Total protein extracts from Sin1 knockdown HeLa cells, showing reduction of Sin1 levels and loss of rictor stability as previously reported. Cells were growing in normal medium 72 h after siRNA transfection and stimulated with 100 nM insulin for 15 min before harvest.

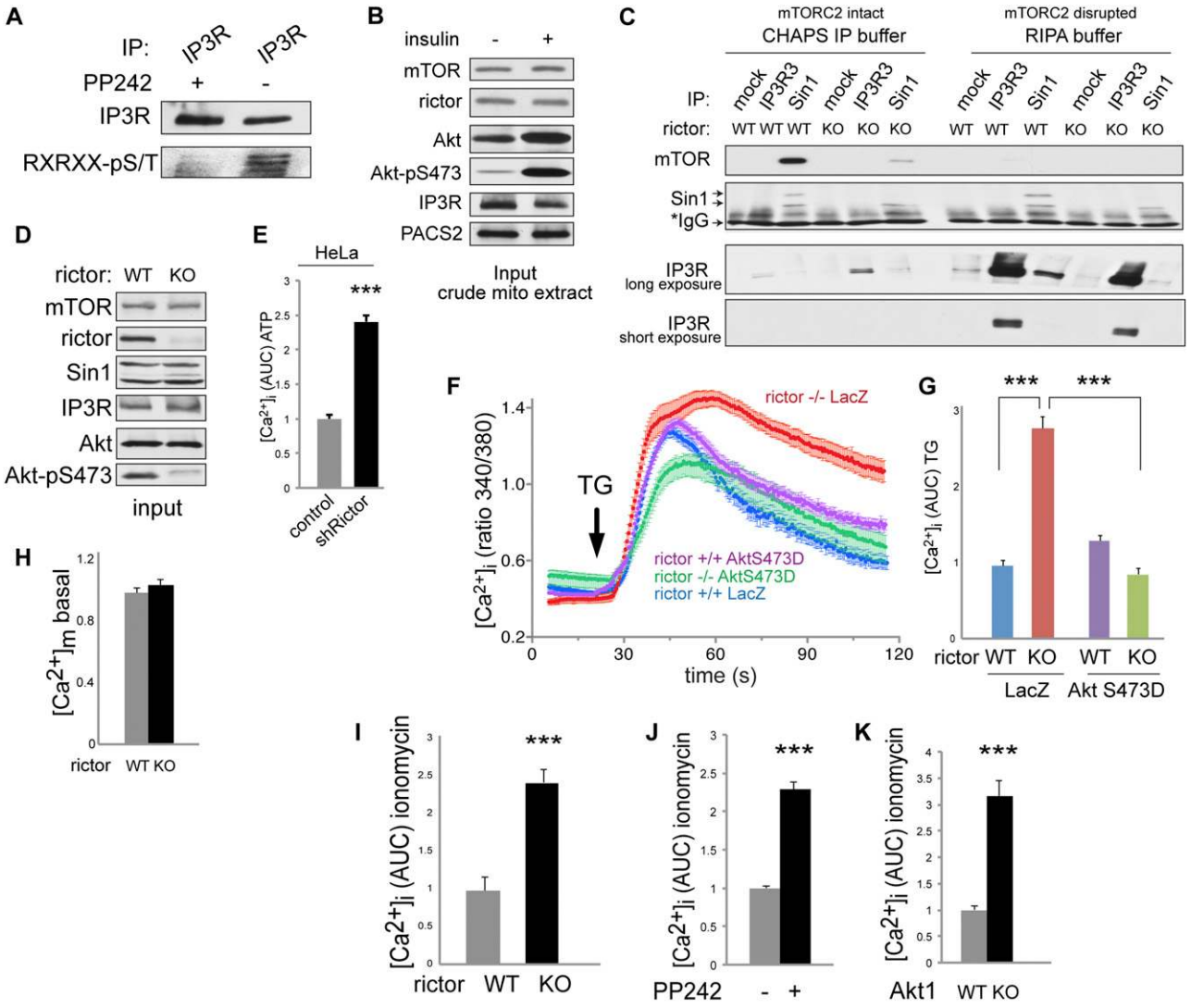

Fig. S5. (*A*) Phosphorylation of IP3R at Akt target site is sensitive to mTOR inhibition. HeLa cells were starved for 14 h, treated with 500 nM PP242 or DMSO for 20 min, and stimulated with 20% (vol/vol) FCS for 20 min. IP3R was immunoprecipitated and blots were probed with an anti-pan-IP3R or an antiphospho-Akt-Substrate (RXRXXpS/T) antibody. (*B*) Input of Fig. 4*C*. Note that starting material for IP was equalized so that equal mTORC2, IP3R, and PACS2 levels were used as input. (*C*) IP of IP3R3 and Sin1 from livers of rictor WT and KO mice. IP was performed either in CHAPS IP buffer, preserving mTORC2 integrity, or in RIPA buffer disrupting mTORC2. In CHAPS buffer, more IP3R3 can be precipitated in rictor KO vs. WT extracts because mTORC2 binding to IP3R3 appears to mask the epitope recognized by the IP antibody. Mice were fed a standard chow diet and killed in the morning. (*D*) Input of *C*. (*E*) AUC of intracellular calcium release in HeLa cells after stimulation with 200 μM ATP, quantified by the emission ratio 340/380 nm after labeling with Fura2-AM. $n = 74–104$. Cells were grown in normal medium before harvest. (*F*) Intracellular calcium release in MEFs expressing LacZ or Akt-S473D after stimulation with 10 μM TG, visualized by Fura2-AM. ($n = 16–54$). For quantification, see *G*. (*G*) AUC of *F*. (*H*) Basal (unstimulated) mitochondrial calcium concentration showing no significant difference between rictor KO and control MEFs growing in normal medium. $n = 20$. (*I*) AUC of intracellular calcium release in rictor KO and control primary hepatocytes after stimulation with 10 μM ionomycin visualized by Fura2-AM ($n = 21–33$), arbitrary units. Hepatocytes were isolated 24 h before measurement. (*J*) AUC of intracellular calcium release in HEK293T cells treated with mTOR inhibitor PP242 after stimulation with 10 μM ionomycin visualized by Fura2-AM ($n = 147–176$), arbitrary units. Cells were grown on chambered culture slides in normal medium in presence of DMSO or 1 μM PP242 for 6 h before measurement. (*K*) AUC of intracellular calcium release in Akt1 KO and control MEFs after stimulation with 10 μM ionomycin visualized by Fura2-AM ($n = 23–25$), arbitrary units. Cells were grown on chambered culture slides in normal medium. Results are shown as mean ± SEM. (*$P < 0.05$; ***$P < 0.001$.)

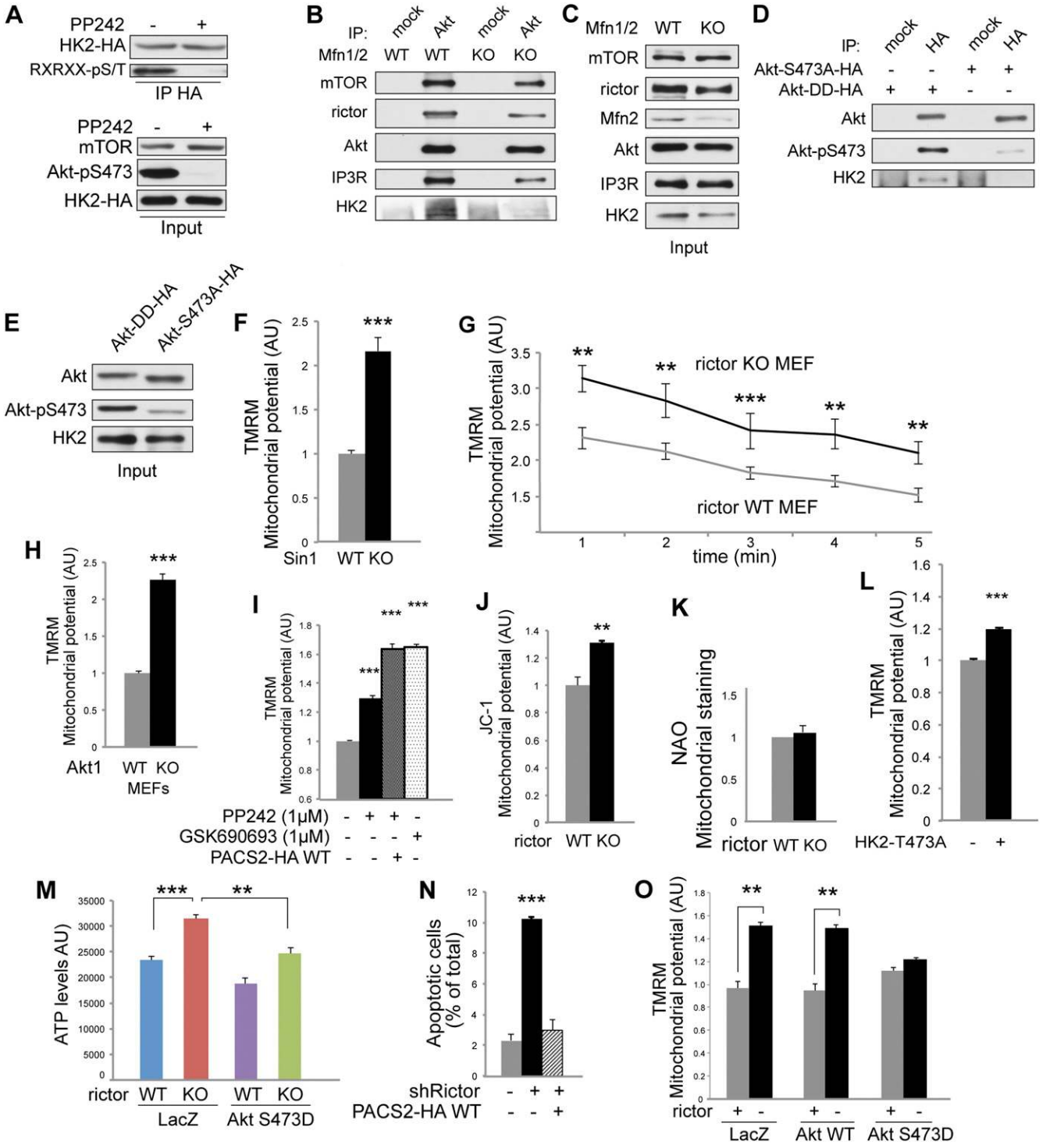

Fig. S6. (*A*) Akt-mediated phosphorylation of HK2. Overexpressed HK2-HA was immunoprecipitated from HeLa cells. Blots were probed with anti-HA or antiphospho-Akt-substrate (RXRXXpS/T) antibody. HK2-HA was immunoprecipitated and probed with a HA-tag or an Akt substrate motif antibody. Thirty-four hours after HK2 transfection, cells were serum-starved for 14 h, treated with 1 μM PP242 for DMSO for 20 min, stimulated with insulin (100 nM) for 15 min, and lysed in RIPA buffer. (*B*) IP of Akt from total protein extracts of MAM-deficient Mfn1/2 and control MEFs. Cells were grown in normal medium and lysed in RIPA buffer. (*C*) Input of *B*. (*D*) IP of overexpressed Akt mutants. Akt-DD is mutated at the sites T308D and AktS473D. Cells were growing in normal medium before lysis in RIPA buffer. (*E*) Input of *D*. (*F*) Mitochondrial potential of Sin1 KO or control MEFs, measured by TMRM intensity by life cell imaging. Arbitrary units, n = 62–69. Cells were grown on chambered slides in normal medium. (*G*) Mitochondrial potential of inducible rictor KO or control MEFs, measured by TMRM intensity by life cell imaging over 5 min. Arbitrary units, n = 17–21. Cells were grown in chambered slides in normal medium. (*H*) Mitochondrial potential of Akt1 KO and control MEFs, measured by TMRM intensity by FACS. Cells were grown in normal medium. (*I*) Mitochondrial potential of HEK293T cells, measured by TMRM intensity by FACS. Cells were serum-starved for 14 h, pretreated with mTOR inhibitor PP242 or Akt inhibitor GSK690693 for 20 min, and stimulated with insulin 100 nM for 30 min during the staining procedure. Where indicated, cells were transfected with wild-type PACS2-HA 48 h before the experiment. Note that PACS2 overexpression does not rescue the effect of mTOR inhibition. (*J*) Mitochondrial potential of inducible rictor KO or control MEFs, measured by

Legend continued on following page

JC-1 intensity by FACS. Arbitrary units, $n = 3$. Cells were grown in normal medium. (*K*) Mitochondrial staining intensity measured by a mitochondrial potential independent dye (NAO), quantified by FACS ($n = 3$). Cells were grown in normal medium. (*L*) Mitochondrial potential HeLa cells upon transfection of HK2-T473A, measured by TMRM intensity by FACS. Cells were grown in normal medium. (*M*) ATP levels of rictor KO and control MEFs infected adenovirally with LacZ or Akt-S473D, measured by CellTiter-Glo luminescence assay ($n = 12$). Cells were grown in normal medium. (*N*) Apoptotic rictor knockdown and control HeLa cells as determined by positive Annexin V staining were analyzed by FACS ($n = 3$). Cells were transfected with a mock or with a plasmid expressing PACS2 48 h before experiment and grown in normal medium. (*O*) Mitochondrial potential of rictor KO and control MEFs infected adenovirally with LacZ, Akt or Akt-S473D, measured by TMRM staining by FACS. Cells were growing in normal medium and infected 48 h before experiment. Results are shown as mean ± SEM and normalized to wild-type cells. $*P < 0.05$, $**P < 0.01$, $***P < 0.001$.

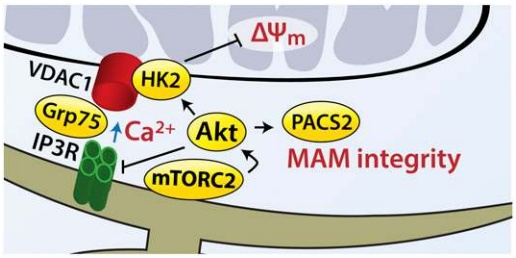

Fig. S7. Model of mTORC2-Akt signaling at MAM. mTORC2 localizes to the ER subdomain MAM. At MAM, mTORC2 can phosphorylate and active Akt. mTORC2-activated Akt can phosphorylate: (*i*) IP3R3, thereby inhibiting its potential to release calcium at MAM; (*ii*) PACS2, thereby controlling MAM integrity; (*iii*) HK2, thereby controlling mitochondrial potential and, thus, energy production.